J. Fluid Mech. (1993), *vol.* 247, *pp.* 369–416

On the instability of hypersonic flow past a flat plate

By NICHOLAS D. BLACKABY[1], STEPHEN J. COWLEY[2] AND PHILIP HALL[1]

[1] Department of Mathematics, The University, Manchester M13 9PL, UK

[2] Department of Applied Mathematics and Theoretical Physics, University of Cambridge, Silver Street, Cambridge CB3 9EW, UK

(Received 30 July 1991 and in revised form 11 August 1992)

The instability of hypersonic boundary-layer flow over a flat plate is considered. The viscosity of the fluid is taken to be governed by Sutherland's formula, which gives a more accurate representation of the temperature dependence of fluid viscosity at hypersonic speeds than Chapman's approximate linear law. A Prandtl number of unity is assumed. Attention is focused on inviscid instability modes of viscous hypersonic boundary layers. One such mode, the 'vorticity' mode, is thought to be the fastest growing disturbance at high Mach numbers, $M \gg 1$; in particular it is believed to have an asymptotically larger growth rate than any viscous instability. As a starting point we investigate the instability of the hypersonic boundary layer which exists far downstream from the leading edge of the plate. In this regime the shock that is attached to the leading edge of the plate plays no role, so that the basic boundary layer is non-interactive. It is shown that the vorticity mode of instability operates on a different lengthscale from that obtained if a Chapman viscosity law is assumed. In particular, we find that the growth rate predicted by a linear viscosity law overestimates the size of the growth rate by $O((\log M)^{\frac{1}{2}})$. Next, the development of the vorticity mode as the wavenumber decreases is described. It is shown, *inter alia*, that when the wavenumber is reduced to $O(M^{-\frac{3}{2}})$ from the $O(1)$ initial, 'vorticity-mode' scaling, 'acoustic' modes emerge.

Finally, the inviscid instability of the boundary layer near the leading-edge interaction zone is discussed. Particular attention is focused on the strong-interaction zone which occurs sufficiently close to the leading edge. We find that the vorticity mode in this regime is again unstable. The fastest growing mode is centred in the adjustment layer at the edge of the boundary layer where the temperature changes from its large, $O(M^2)$, value in the viscous boundary layer, to its $O(1)$ free-stream value. The existence of the shock indirectly, but significantly, influences the instability problem by modifying the basic flow structure in this layer.

1. Introduction

Our concern is with the instability of hypersonic boundary-layer flows. In the first instance we will consider flows where the influence of shocks is negligible, and then we will show how the instability problem can be significantly modified by shock effects. The motivation for this and related work on hypersonic boundary-layer instability theory is the renewed interest in hypersonic flight which has been stimulated by plans to build the National Aerospace Plane (X-30). A primary

concern with such vehicles is the question of where transition will occur over a wide range of Mach numbers and whether it can be controlled. At the largest relevant Mach numbers, say Mach 20–25, the extremely high temperatures associated with the flow would destroy the vehicle unless it were cooled, so that it is of interest to identify the effect wall temperature has on flow instability.

The purpose of this paper is to determine qualitative features of the inviscid instability characteristics of hypersonic boundary-layer flows. We recall that there is a simple generalization of Rayleigh's (incompressible) inflexion point theorem to compressible flows (Lees & Lin 1946), and that most compressible boundary layers turn out to be inviscidly unstable even though their incompressible counterparts are stable. This is a significant result because, at sufficiently large Reynolds numbers, the growth rates of inviscid disturbances tend to be much larger than those of viscous instabilities; thus they are prime candidates for causing transition to turbulence in many situations. The modes discussed in this paper might be referred to as generalized-inflexion-point modes because the phase speed of the neutral mode (actually the *upper-branch* neutral mode), is equal to the fluid velocity at the generalized inflexion point. Furthermore the eigenfunctions of the fastest growing modes are localized around that inflexion point.

For convenience we will concentrate on high-Reynolds-number flow past a flat plate, although many aspects of our analysis are applicable to other boundary-layer flows either directly or by straightforward extension (e.g. flow past a wedge or cone). Throughout we assume that the fluid is Newtonian, and that its viscosity is adequately described by Sutherland's formula. We will also take the Prandtl number to be one. This simplifies the analysis since a first integral of the energy equation for the underlying steady flow exists. The assumption of unit Prandtl number is not unduly restrictive as far as understanding the properties of the fastest growing mode is concerned, and results in a more elegant analysis. However, as Grubin & Trigub (1993*a*, *b*) show in their independent and closely related study, the properties of small-growth-rate modes with wavelengths much longer than the thickness of the boundary layer can depend delicately on the Prandtl number (see §3.3 for further discussion, and Jackson & Grosch 1991 for numerical calculations concerning shear layers). Also, while we assume that the Mach number is large, the complications arising from real gas effects are not investigated; Fu, Hall & Blackaby (1990) considered real gas effects on the Görtler vortex instability mechanism, with no shock present, and concluded that they have little direct influence at the top of the boundary layer, where the disturbance is concentrated.

Reshotko (1976) and Mack (1987) have reviewed work on the linear instability of high-Reynolds-number compressible flows. Many of these studies are based on the compressible extension of the Orr–Sommerfeld equation; for a critique of the mathematical rigour of this approach see Smith (1979, 1989). Here we examine the linear stability of high-Reynolds-number flows by means of formal asymptotic expansions. This approach was that originally used by Heisenberg (1924), Tollmien (1929) and Lin (1945*a*–*c*) to study boundary-layer stability. More recently, for example, Smith (1989) has refined their approach by applying triple-deck theory to lower-branch, viscous, Tollmien–Schlichting modes of compressible boundary layers. Seddougui, Bowles & Smith (1991) have extended this theory to include the effects of severe wall cooling. Cowley & Hall (1990, hereafter referred to as CH), have shown how such modes can interact with a shock at large Mach number, while Seddougui & Bassom (1991) have looked at a weakly nonlinear version of this problem. However, viscous modes have relatively small rates at sufficiently large Reynolds

numbers, and our main concern will be with the faster growing inviscid modes. As a result, our analysis is based on asymptotic scalings which lead to the Rayleigh equation rather than the triple-deck equations. We note that the third type of instability responsible for boundary-layer transition, the Görtler vortex mode, develops an asymptotic structure at high Mach numbers closely related to that of our inviscid modes – see Hall & Fu (1989) and Fu *et al.* (1990) for the Chapman-law and Sutherland-formula versions respectively.

When a quasi-parallel approximation is formally justifiable because the Reynolds number is large, inviscid modes satisfy the compressible generalization of Rayleigh's equation. Numerical solutions to this equation have been reported by, *inter alios*, Mack (1969, 1984, 1987) for boundary-layer flows, Jackson & Grosch (1989, 1991) for shear flows, and Papageorgiou (1990) for wake flows. For fluids satisfying a Chapman viscosity law, high-Mach-number asymptotic solutions to this equation for one type of so-called 'acoustic' boundary-layer modes have been obtained by CH, while Smith & Brown (1990, hereafter referred to as SB), have identified the asymptotic form of the 'vorticity' mode – including an exact solution of the governing equation. Balsa & Goldstein (1990) and Papageorgiou (1991) have given asymptotic descriptions for the high-Mach-number inviscid instability of shear layers and wakes, respectively, assuming a Chapman-law fluid. Though the flows investigated by SB, Balsa & Goldstein (1990) and Papageorgiou (1991) differ, the analysis results in the same eigenvalue problem for the vorticity mode. This is because the vorticity mode is trapped in a thin layer where the overall features of the basic flow are unimportant.

In the above-mentioned boundary-layer analyses, and also in the hypersonic Görtler vortex instability analysis of Hall & Fu (1989), one of the key asymptotic regions for the case of a Chapman viscosity law is a *logarithmically* thin 'adjustment' layer which develops due to the *exponential* decay of the underlying steady temperature field away from the wall. However, Chapman's viscosity law is not exact, and was introduced as a useful interpolation law which greatly simplified steady boundary-layer calculations; for example Stewartson (1955) hoped that the use of idealized physical properties would help in understanding 'the behaviour of more realistic fluids'. At the large temperatures typical in hypersonic flows, Chapman's law differs significantly from both the more precise Sutherland's formula and the viscosity–temperature power-law formula. In fact, because Chapman's law is simply a linear approximation to the viscosity–temperature dependence of the fluid, it is of questionable validity in the hypersonic limit.

At high Mach numbers the steady temperature field in a fluid satisfying Sutherland's viscosity formula (or a power-law formula) initially decays algebraically away from the wall, before reverting to exponential decay in an asymptotic region 'far' from the wall (e.g. Freeman & Lam 1959). This algebraic decay changes the scalings in the adjustment region; in particular the asymptotic expansions proceed purely in inverse powers of M rather than in inverse powers of both $(\log(M))^{\frac{1}{2}}$ and M. Moreover the wavelength of the most unstable disturbance varies by a factor of $(\log(M))^{\frac{1}{2}}$ in the two cases. We note that a similar difference in scalings is evident in the interaction region of steady hypersonic flow past a flat plate. In that case Lee & Cheng (1969) have shown that the shock-heating adjustment layer is logarithmically thin for Chapman's viscosity law, whereas for a power-law viscosity formula, and hence for Sutherland's formula, the scaling for the adjustment layer is algebraic in nature (Bush 1966).

The flows that we consider here are appropriate to different downstream locations for hypersonic flow past a semi-infinite plate. In the first instance we shall consider

the instability of a non-interactive flow. This is appropriate to large distances downstream of the leading edge of the plate, where the attached shock at the leading edge has no effect on the flow field. This basic state, and the Rayleigh equation which is shown to govern its inviscid instability, are discussed in §2. The dispersion relation associated with the Rayleigh equation is then derived in §3. We discuss the growth rate of the mode over the whole range of unstable wavenumbers and show how the vorticity mode, acoustic modes and Tollmien–Schlichting modes are all inter-related. A similar non-interactive flow field is also considered by Grubin & Trigub (1993*a*, *b*). They assume a fluid with a power-law viscosity, and allow for a broader range of Prandtl numbers.

Then in §4 we go on to discuss the basic state in the 'interaction zone' further upstream (see figure 8 for a schematic of the steady flow in this region). Since Sutherland's viscosity formula reduces to a so-called 'power-law' at large temperatures, the description of the underlying steady flow here is essentially that for a power-law fluid due to Luniev (1959) and Bush (1966). They showed that the 'interactive' region occurs for $R = O(M^5)$, where R is the Reynolds number based on distance from the leading edge. Although the resulting system of equations can only be solved numerically, it is still possible to consider the instability of the flow in this region, and we derive appropriate (quasi-parallel) stability equations. The 'strong' hypersonic interaction limit then corresponds to letting the streamwise variable tend to zero on the $R = O(M^5)$ scale. In that limit a similarity solution for the basic flow can be found (Bush 1966), and a re-scaled Rayleigh equation for the disturbance is derived. The solution of that equation is discussed in §5. Note that we could have instead considered the weak hypersonic limit further downstream; we also note that this weak hypersonic limit is different from the 'non-interactive' limit discussed in §2. In particular, the 'entropy' layer generated by the leading-edge shock is not assumed to have merged into the viscous boundary layer in the weak limit (cf. Reshotko & Khan 1979), whereas it is assumed to have merged in the 'very-far' downstream non-interactive limit considered in §2 (see also Bush & Cross 1967). We choose to concentrate on the strong-interaction regime because, it is, to a certain extent, simpler. Further, if the flow is unstable in this regime it is arguable that growing disturbances will originate here and lead to transition. In §6 we give a summary and numerical comparison, and conclude with a discussion in §7.

2. Non-interactive steady flows

We begin by considering the stability of steady hypersonic flow far downstream from any leading-edge interaction zone; in particular, if L is the distance from the leading edge, and $\hat{U}_\infty$, $\hat{a}_\infty$, $\hat{\rho}_\infty$ and $\hat{\mu}_\infty$, are the velocity, sound speed, density and shear viscosity of the free-stream flow, then we assume that the Reynolds number,

$$R = \hat{\rho}_\infty \hat{U}_\infty L/\hat{\mu}_\infty \tag{2.1a}$$

is larger than whatever power of the Mach number,

$$M = \hat{U}_\infty/\hat{a}_\infty, \tag{2.1b}$$

is necessary for interactive and/or non-parallel effects to be negligible (see the sentence following criterion (3.29) for a more precise restriction). We adopt a non-dimensionalization based on coordinates $L\boldsymbol{x}$ (where x is in the direction of flow and y is normal to plate), velocities $\hat{U}_\infty \boldsymbol{u}$, time $Lt/\hat{U}_\infty$, pressure $\hat{\rho}_\infty \hat{U}_\infty^2 p$, density $\hat{\rho}_\infty \rho$,

temperature $\hat{T}_\infty T$, and shear and bulk viscosities $\hat{\mu}_\infty \mu$ and $\hat{\mu}_\infty \mu'$ respectively, where the subscript ∞ denotes the value of the quantity in the free stream. On the assumption that the fluid is a perfect gas with a constant ratio of specific heats, γ, the governing equations of the flow are

$$\frac{\partial \rho}{\partial t} + \boldsymbol{\nabla} \cdot (\rho \boldsymbol{u}) = 0, \tag{2.2a}$$

$$\rho \frac{\mathrm{D}\boldsymbol{u}}{\mathrm{D}t} = -\boldsymbol{\nabla} p + \frac{1}{R}(2\boldsymbol{\nabla} \cdot (\mu \boldsymbol{e}) + \boldsymbol{\nabla}((\mu' - \tfrac{2}{3}\mu)\,\boldsymbol{\nabla} \cdot \boldsymbol{u})), \tag{2.2b}$$

$$\rho \frac{\mathrm{D}T}{\mathrm{D}t} = (\gamma - 1) M^2 \frac{\mathrm{D}p}{\mathrm{D}t} + \frac{1}{Pr\,R} \boldsymbol{\nabla} \cdot (\mu \boldsymbol{\nabla} T) + \frac{(\gamma - 1) M^2}{R} \Phi, \tag{2.2c}$$

$$\gamma M^2 p = \rho T, \tag{2.2d}$$

where

$$e_{ij} = \frac{1}{2}\left(\frac{\partial u_i}{\partial x_j} + \frac{\partial u_j}{\partial x_i}\right), \tag{2.3a}$$

$$\Phi = 2\mu \boldsymbol{e} : \boldsymbol{e} + (\mu' - \tfrac{2}{3}\mu)\,(\boldsymbol{\nabla} \cdot \boldsymbol{u})^2, \tag{2.3b}$$

and Pr is the constant Prandtl number. For a shear viscosity obeying Sutherland's formula

$$\mu = \left(\frac{1 + \check{C}}{T + \check{C}}\right) T^{\frac{3}{2}}, \tag{2.3c}$$

where $\check{C} \approx 110.4 \hat{T}_\infty^{-1}$ for air temperatures measured in degrees Kelvin. In the numerical calculations discussed below we took $\hat{T}_\infty = 216.9$ as a 'typical' temperature in the upper atmosphere, leading to the value $\check{C} = 0.509$. The bulk viscosity μ' does not appear in the inviscid-stability equations derived later in this paper.

The boundary-layer equations can be recovered (e.g. see Stewartson 1964) by first substituting

$$\hat{\eta} = R^{\frac{1}{2}} \int_0^y \rho \, \mathrm{d}y, \quad v = R^{-\frac{1}{2}} V, \tag{2.4a, b}$$

where $\hat{\eta}$ is the Dorodnitsyn–Howarth variable, and then taking the limit $R \to \infty$.

For steady two-dimensional flow over a flat plate with leading edge at $x = 0$, a similarity solution to these equations exists. With

$$\eta = \hat{\eta} / [(1 + \check{C})\, x]^{\frac{1}{2}}, \quad u = \psi_{\hat{\eta}}, \quad \rho V = -(\psi_x + \hat{\eta}_x \psi_{\hat{\eta}}), \tag{2.5a}$$

$$\psi = [(1 + \check{C})\, x]^{\frac{1}{2}} f(\eta), \quad T \equiv T(\eta), \quad \rho \equiv \rho(\eta), \quad p = \frac{1}{\gamma M^2}, \tag{2.5b}$$

the governing equations are found to be

$$\rho T = 1, \quad \tfrac{1}{2} f f'' + \left(\frac{T^{\frac{1}{2}}}{T + \check{C}} f''\right)' = 0, \tag{2.6a, b}$$

$$\tfrac{1}{2} f T' + \frac{1}{Pr}\left(\frac{T^{\frac{1}{2}}}{T + \check{C}} T'\right)' + \frac{(\gamma - 1) M^2 T^{\frac{1}{2}}}{T + \check{C}} f''^2 = 0, \tag{2.6c}$$

subject to the boundary conditions

$$f(0) = f'(0) = 0, \quad f'(\infty) = T(\infty) = 1, \tag{2.6d}$$

and $T(0) = T_w$ (fixed wall-temperature) or $T'(0) = 0$ (insulated wall). (2.6*e*)

Here primes denote differentiation with respect to η. For simplicity we will focus attention on $Pr = 1$, and denote by T_r the adiabatic wall temperature (see Grubin & Trigub (1993*a*, *b*) for the $Pr \neq 1$ case). Then, as is well known (e.g. Stewartson 1964), the energy equation can be integrated to yield

$$T = 1 + ((T_b - 1) + \tfrac{1}{2}(\gamma - 1)M^2(T_b + f'))(1 - f'), \tag{2.7}$$

where $T_w = T_b T_r$ and $T_r = 1 + \frac{1}{2}(\gamma - 1)M^2$.

The solution to (2.6) in the limit of large Mach number has been examined by Freeman & Lam (1959) and Bush & Cross (1967). They showed that two asymptotic regions develop, distinguished by the positions where the coordinates η and $\xi = M^{\frac{1}{2}}\eta$, respectively, are order one.

2.1. *The high-temperature region*: $\xi = O(1)$

In this region we write $f = M^{-\frac{1}{2}} f_0(\xi) + \ldots$, then using (2.7) it follows from (2.6*b*) that

$$f_0 f_0'' + \left(\frac{8}{\gamma - 1}\right)^{\frac{1}{2}} \left(\frac{f_0''}{(T_b + f_0')^{\frac{1}{2}}(1 - f_0')^{\frac{1}{2}}}\right)' = 0, \tag{2.8a}$$

with $$f_0(0) = f_0'(0) = 0, \tag{2.8b}$$

and $$f_0 \sim \xi + \bar{A} + \frac{24}{(T_b + 1)(\gamma - 1)\xi^3} - \frac{72\bar{A}}{(T_b + 1)(\gamma - 1)\xi^4} + \ldots \quad \text{as} \quad \xi \to \infty, \tag{2.8c}$$

where the constant $\bar{A}$ must be determined numerically. Throughout the paper detailed expansions are given for the solutions at the edges of asymptotic regions; this is because the algebraic nature of the expansions often means that more than the leading-order term is required to obtain accurate numerical results. The algebraic decay is of course different from the case of a Chapman-law fluid for which the expansions contain exponentially small terms. For future reference observe (*a*) that in this region $T = O(M^2)$, and hence Sutherland's formula reduces to a power-law form at leading order, and (*b*) that from (2.4*a*) the boundary-layer thickness in this region is $O(M^{\frac{3}{2}})$, and is thus relatively large (see figure 1*a*).

2.2. *The temperature adjustment region*: $\eta = O(1)$

Here, with

$$f = \eta + \bar{A}/M^{\frac{1}{2}} + \bar{f}_1/M^2 + \ldots, \tag{2.9}$$

we find that the perturbation $\bar{f}_1$ satisfies the nonlinear equation

$$\eta \bar{f}_1'' + 2\left(\frac{[1 - \frac{1}{2}(\gamma - 1)(T_b + 1)\bar{f}_1']^{\frac{1}{2}}}{1 + \bar{C} - \frac{1}{2}(\gamma - 1)(T_b + 1)\bar{f}_1'} \bar{f}_1''\right)' = 0, \tag{2.10a}$$

subject to

$$\bar{f}_1 \sim \frac{24}{(T_b + 1)(\gamma - 1)\eta^3} \quad \text{as} \quad \eta \to 0, \quad \text{and} \quad \bar{f}_1 \to 0 \quad \text{as} \quad \eta \to \infty. \tag{2.10b}$$

In this region $T = O(1)$, and thus the full form of Sutherland's formula holds. Although this temperature-adjustment layer is thicker than the higher-temperature region in terms of the Dorodnitsyn–Howarth similarity variable η, it follows from (2.4*a*) that in physical coordinates it is a thin layer of $O(1)$ thickness sitting atop the much wider $O(M^{\frac{3}{2}})$ high-temperature boundary layer.

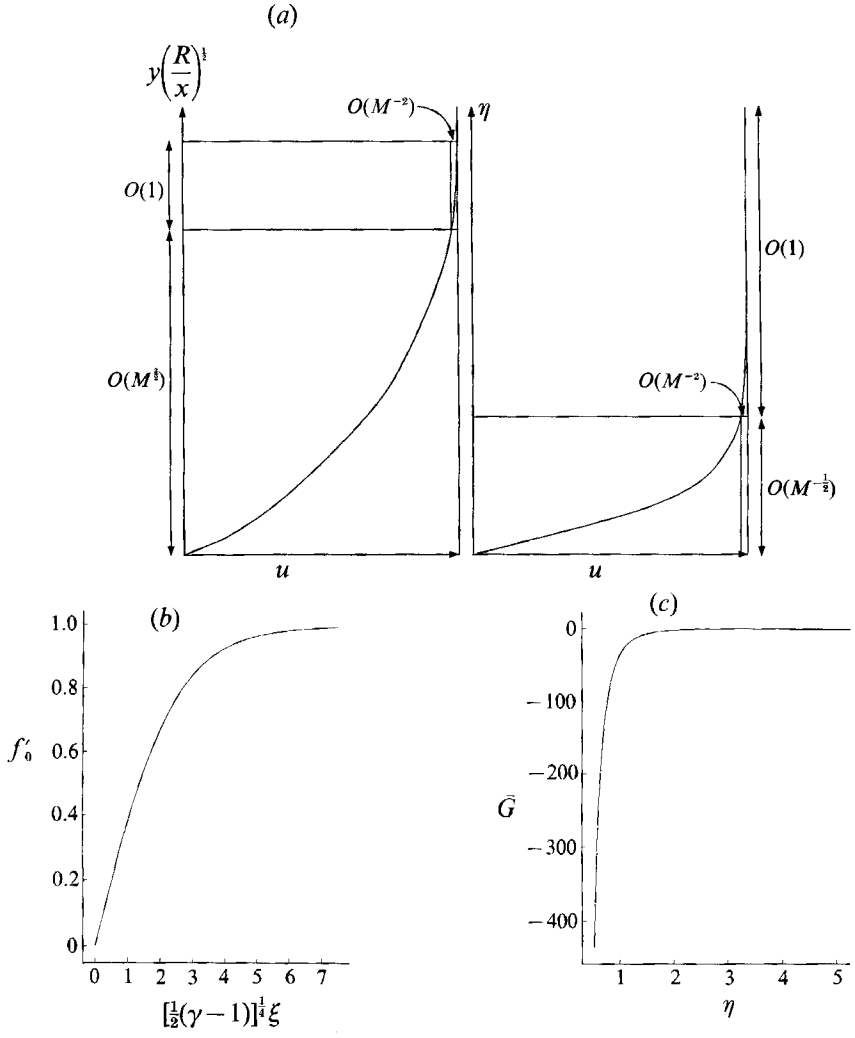

FIGURE 1. (*a*) Schematic illustration of the thickness of the high-temperature region and the adjustment region of the boundary layer in physical and Dorodnitsyn–Howarth variables. (*b*) The solution of the wall-layer equation (2.8*a*) for the adiabatic case $T_b = 1$ with $\gamma = 1.4$ and $\tilde{C} = 0.509$. (*c*) The solution of the adjustment-layer equation (2.10*c*) for the case $\tilde{C} = 0.509$.

In order to illustrate the underlying velocity profiles, in figure 1 (*b*) we have plotted the function f_0' against $((\gamma-1)/2)^{\frac{1}{4}}\xi$ for the adiabatic case $T_b = 1$, and then in figure 1 (*c*) we have plotted the adjustment-layer function

$$\bar{G} = \tfrac{1}{2}(T_b+1)(\gamma-1)\bar{f}_1', \tag{2.10c}$$

against η; $\bar{G}$ is independent of T_b and γ. The figures illustrate the respective algebraic and exponential decay of the two velocity profiles away from the wall. It is also worth pointing out that for a Chapman-law fluid the adjustment-layer equation corresponding to (2.10*a*) is linear, and that its solution can be expressed in terms of the exponential function. It is this simplification that enabled SB to spot the exact solution of the neutral vorticity mode in their study of instabilities in this layer. We have been unable to find an exact solution of the analogous stability equation for Sutherland's formula.

2.3. *Rayleigh's equation*

We now investigate the stability of this non-interactive steady flow. Sufficiently far downstream the quasi-parallel assumption is valid for inviscid instability modes. It is then appropriate to seek perturbations of the form

$$(u,p) = \left(f'(\eta), \frac{1}{\gamma M^2}\right) + \ldots + \Delta(\tilde{u}(\eta), \tilde{p}(\eta)) \exp\left(\mathrm{i}R^{\frac{1}{2}}\theta(x,z,t)\right) + \ldots, \quad (2.11a,b)$$

with similar expressions for the other flow quantities. Here Δ is the small disturbance amplitude, and as is conventional, we define local wavenumbers, a local frequency and a local wave speed by

$$(\alpha,\beta,\omega) = [(1+\check{C})x]^{\frac{1}{2}}(\theta_x, \theta_z, -\theta_t), \quad c = \omega/\alpha. \quad (2.11c,d)$$

If Δ is sufficiently small, substitution into (2.2) demonstrates that the pressure perturbation $\tilde{p}$ satisfies the linear, compressible, Rayleigh equation:

$$\frac{\mathrm{d}^2\tilde{p}}{\mathrm{d}\eta^2} - \frac{2f''}{f'-c}\frac{\mathrm{d}\tilde{p}}{\mathrm{d}\eta} - (\alpha^2+\beta^2)\,T\left(T - \frac{\alpha^2M^2(f'-c)^2}{\alpha^2+\beta^2}\right)\tilde{p} = 0. \quad (2.12a)$$

The conditions that there is no normal velocity at the wall, and that the disturbance is confined to the boundary layer, can be expressed as

$$\tilde{p}' = 0 \quad \text{on} \quad \eta = 0, \quad \tilde{p} \to 0 \quad \text{as} \quad \eta \to \infty. \quad (2.12b)$$

Here we have assumed that the instability modes are confined to the boundary layer. We do not consider modes which have the form of outgoing sound waves far from the boundary, or, in the case of instability waves that reflect at a shock, modes which include both incoming and outgoing waves far from the boundary (e.g. see CH).

Equation (2.12a) and boundary conditions (2.12b) determine a temporal stability eigenrelation if α and β are taken to be real; alternatively they determine a spatial stability eigenrelation if αc and β are taken to be real.

3. The far downstream behaviour of the inviscid modes

In this section we discuss the asymptotic form of unstable solutions to (2.12a) for the region far downstream of the leading edge of the plate. In a previous investigation CH studied aspects of the so-called 'acoustic' modes of (2.12a) in this region using Chapman's viscosity law. Simultaneously SB investigated the vorticity mode using Chapman's law. The main difference between these two types of modes is that the 'acoustic' modes have wavelengths comparable with the thickness of the boundary layer, i.e. $(\alpha,\beta) = O(M^{-2})$, whilst the vorticity mode, at least close to the upper branch, has a much larger wavenumber, i.e. $(\alpha,\beta) = O((2\log M^2)^{\frac{1}{2}})$. Moreover the vorticity mode is concentrated in the adjustment layer at the edge of the boundary layer (see §2.2), whilst the acoustic one is distributed over the physically much larger main part of the boundary layer (see §2.1).

However, as indicated above, at high Mach numbers the temperature variations in the boundary layer are large. Thus a linear temperature–viscosity law is an unsuitable approximation, and Sutherland's formula or a power-law formula should be used to give a better representation of the viscosity. It is then important to see how the asymptotic structures developed by CH and SB change.

In the first instance we derive an asymptotic solution for a vorticity mode of (2.12a). We determine the neutral values of α, β and c for this mode, and find the

limiting form of the mode when the small-wavenumber limit $(\alpha, \beta) \to 0$ is taken. This limiting solution points to a sequence of distinguished asymptotic limits. These are a little messy algebraically, and hence for an overview the reader may find it useful to refer to the schematic plot of temporal growth rate against wavenumber given in figure 7. Within this sequence of asymptotic limits the scaling, $(\alpha, \beta) = O(M^{-\frac{3}{2}})$, appropriate to 'acoustic' modes emerges; we therefore discuss these modes as a limiting case of the long-wavelength 'vorticity' mode. In addition we indicate why sufficiently oblique, long-wavelength, Rayleigh modes can alternatively be viewed as short-wavelength Tollmien–Schlichting waves.

3.1. *Modes with wavelengths comparable with the thickness of the adjustment region: $(\alpha, \beta) = O(1)$. The vorticity mode*

Consider then the solution of (2.12*a*) which has the eigenfunction trapped in the temperature-adjustment layer at the edge of the boundary layer. We seek a solution which has $(\alpha, \beta) = O(1)$, so that the wavelength of the vorticity mode is comparable with the width of the physically thin adjustment layer. From (2.5), (2.7), (2.9) and (2.10*c*) the velocity field, $\bar{u}$, and temperature field, $\bar{T}$, of the underlying steady flow expand as

$$\bar{u} = 1 + \frac{2\bar{G}(\bar{\eta})}{(\gamma-1)(T_b+1)M^2} + \ldots, \quad \bar{T} = 1 - \bar{G} + \ldots, \tag{3.1a, b}$$

where $\eta = \sqrt{2}\bar{\eta}$, and $\bar{G}$ has the asymptotic behaviour

$$\bar{G} = -\frac{9}{\bar{\eta}^4} + \frac{B}{\bar{\eta}^{3-\sqrt{7}}} + (2\check{C}+1) + \ldots \quad \text{as} \quad \bar{\eta} \to 0, \tag{3.2a}$$

$$\bar{G} \to 0 \quad \text{exponentially as} \quad \bar{\eta} \to \infty. \tag{3.2b}$$

Here B is a constant which has to be calculated numerically; $B = -1.81447$ for our choice of the Sutherland constant, $\check{C} = 0.509$.

Next we expand α, β, c and $\tilde{p}$ in the forms

$$(\alpha, \beta) = \frac{1}{\sqrt{2}}(\hat{\alpha}, \hat{\beta}) + \ldots, \quad c = 1 + \frac{2}{(\gamma-1)(T_b+1)M^2}\hat{c} + \ldots, \quad \tilde{p} = \hat{p} + \ldots, \tag{3.3a–c}$$

where we have assumed that the disturbance moves downstream with the fluid speed in the adjustment layer. On substituting for $\bar{u}$ and $\bar{T}$ from (3.1), and using (3.3), we find that the zeroth-order approximation to (2.12*a*) in the adjustment layer is

$$\frac{\mathrm{d}^2\hat{p}}{\mathrm{d}\bar{\eta}^2} - \frac{2\bar{G}'}{\bar{G}-\hat{c}}\frac{\mathrm{d}\hat{p}}{\mathrm{d}\bar{\eta}} - \hat{k}^2(1-\bar{G})^2\hat{p} = 0, \tag{3.4a}$$

where

$$\hat{k} = (\hat{\alpha}^2 + \hat{\beta}^2)^{\frac{1}{2}}. \tag{3.4b}$$

Equation (3.4) is to be solved subject to $\hat{p}$ vanishing in the limits $\bar{\eta} \to 0$ and $\bar{\eta} \to \infty$, i.e. the disturbance is to be confined to the adjustment layer. For $\bar{\eta} \gg 1$ it follows from (3.4) that $\hat{p}$ decays like $\exp(-\hat{k}\bar{\eta})$, whilst for $\bar{\eta} \ll 1$ a WKBJ solution of (3.4) can be expressed in the form

$$\hat{p} \sim \exp\left(-\int \Theta(\bar{\eta})\,\mathrm{d}\bar{\eta}\right), \tag{3.5}$$

where

$$\Theta \sim -\frac{9\hat{k}}{\bar{\eta}^4} + \frac{2}{\bar{\eta}} + \frac{B\hat{k}}{\bar{\eta}^{3-\sqrt{7}}} + 2\check{C}\hat{k} + \ldots \quad \text{as} \quad \bar{\eta} \to 0. \tag{3.6}$$

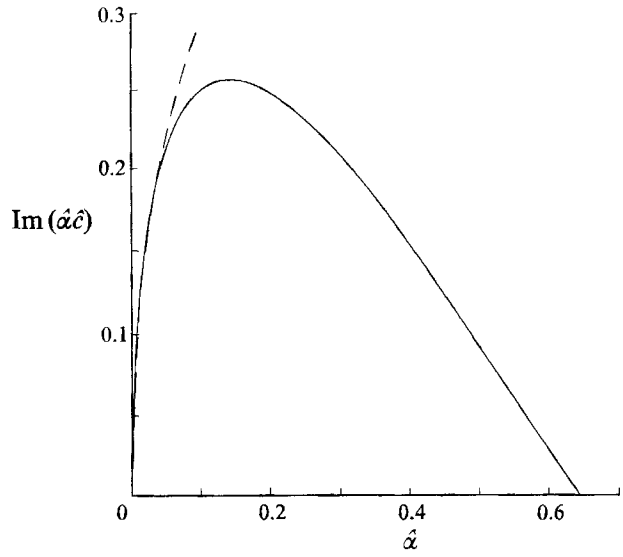

FIGURE 2. The dependence of the vorticity-mode growth rate $\mathrm{Im}\,(\hat{\alpha}\hat{c})$ on the wavenumber $\hat{\alpha}$. The dashed curve represents the asymptotic prediction (3.9) and (3.13*b*).

First, we restrict our attention to the neutral case. The relative wave speed $\hat{c}$ is then real and can be evaluated by finding the fluid speed correct to order M^{-2} at the generalized inflexion point where

$$\frac{\bar{u}_{\eta\eta}}{\bar{u}_{\eta}}-\frac{2\bar{T}_{\eta}}{\bar{T}}=0, \quad \text{i.e. where} \quad \frac{\bar{G}''}{\bar{G}'}+\frac{2\bar{G}'}{1-\bar{G}}=0. \tag{3.7a, b}$$

A numerical solution to (2.10*a*) using a Runge–Kutta method shows that this occurs at $\bar{\eta}\approx 1.604924$, in which case $\hat{c}\approx -0.993937$. The corresponding real value of $\hat{k}$ is obtained by integrating (3.4) from $\bar{\eta}=0$ to $\bar{\eta}=\infty$. In order to avoid difficulties at the generalized inflexion point, the path of integration was deformed into the complex $\bar{\eta}$-plane by taking a triangular contour around and below the inflexion point. Such a calculation predicts that the neutral wavenumber is $\hat{k}\approx 0.645065$.

However, of greater significance are the unstable eigenmodes. First, we consider the results for the case of temporal instability; these are obtained from a numerical solution of (3.4*a*) with the boundary conditions (3.5) and (3.6). Figure 2 illustrates the dependence of the scaled, temporal growth rate, $\mathrm{Im}\,(\hat{\alpha}\hat{c})$, on the scaled, real wavenumber $\hat{\alpha}$ for two-dimensional modes. The maximum scaled, temporal growth rate, $\mathrm{Im}\,(\hat{\alpha}\hat{c})\approx 0.256853$, occurs at $\hat{\alpha}\approx 0.143619$. Further, it follows from the functional form of $\hat{c}$, i.e. $\hat{c}\equiv\hat{c}(\hat{k})$, and Squire's theorem, that three-dimensional modes have smaller (temporal) growth rates, as do 'acoustic' modes (see §3.2 and the Appendix). Hence this two-dimensional mode is the most (temporally) unstable inviscid mode for a hypersonic boundary layer. We note that $\hat{c}$ as defined above is independent of T_{b} and γ, and that from (2.11) and (3.3*b*) the non-dimensionalized (temporal) growth rate is

$$\frac{\sqrt{2}R^{\frac{1}{2}}\,\mathrm{Im}\,(\hat{\alpha}\hat{c})}{[(1+\check{C})x]^{\frac{1}{2}}(\gamma-1)(T_{\mathrm{b}}+1)M^2}.$$

Thus wall cooling, i.e. $0<T_{\mathrm{b}}<1$, has a destabilizing effect on the vorticity mode to

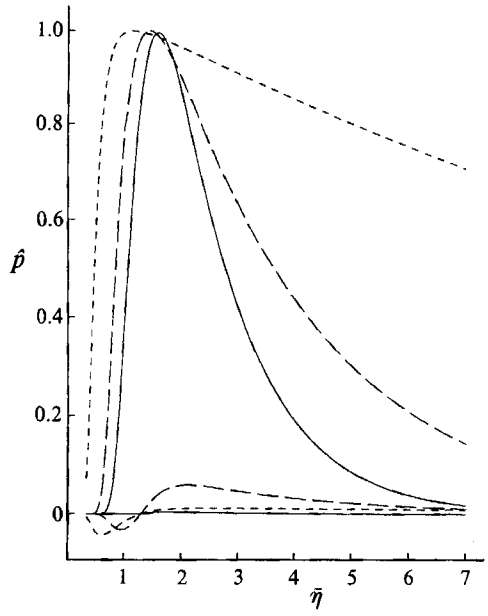

FIGURE 3. The real and imaginary parts of the vorticity-mode eigenfunction at three different values of the wavenumber: ——, $\hat{k} = 0.64$; — —, $\hat{k} = 0.30$; ---, $\hat{k} = 0.05$. The upper three curves correspond to the real parts for the normalization chosen here.

the extent that the temporal growth rate can be doubled by reducing the wall temperature sufficiently.

To consider the spatial instability case, i.e. ω, β real and α complex, an extra term in the expansion of (3.3*a*) is required; thus we expand $\hat{\alpha}$ and $\hat{k}$ as

$$\hat{\alpha} = \frac{\hat{\alpha}_0}{\sqrt{2}} + \frac{\sqrt{2}}{(\gamma-1)(T_b+1)M^2}\hat{\alpha}_1 + \ldots, \quad \hat{k} = \hat{k}_0 + \frac{\hat{k}_1}{M^2} + \ldots, \tag{3.8a, b}$$

where $\hat{k}_0 = (\hat{\alpha}_0^2 + \hat{\beta}^2)^{\frac{1}{2}}$, $\hat{\beta} = \sqrt{2}\beta$, and there is no need to scale the real frequency ω. On substitution into (2.12*a*), (3.4*a*) is again found to govern the stability properties if $\hat{k}$ is replaced by $\hat{k}_0$. It follows from (2.11*d*) and (3.8*a*, *b*) that

$$\hat{\alpha}_0 = \omega, \quad \hat{\alpha}_1 = -\hat{\alpha}_0 \hat{c}. \tag{3.8c}$$

The scaled, spatial growth rate, $\mathrm{Im}(-\hat{\alpha}_1)$, is thus identical to the scaled, temporal growth rate $\mathrm{Im}(\hat{\alpha}\hat{c})$ (see also Balsa & Goldstein 1990). This is a direct consequence of the vorticity modes being 'near neutral' in the sense that they propagate with approximately the free-stream velocity. Thus the spatial instability properties can be immediately deduced from those for the temporal case. In particular, wall cooling has a destabilizing effect and two-dimensional modes are the most unstable.

In figure 3 we show the normalized, complex-valued, eigenfunction of the vorticity-mode equation at different values of the wavenumber. This figure indicates that as the wavenumber decreases, the eigenfunction starts to expand out of the adjustment layer. Thus, if the wavelength increases sufficiently the possibility arises of the disturbance extending outside the boundary layer, and hence of it interacting with external flow features such as shocks. Further, the form of the growth rate at small wavenumbers is of interest because, for sufficiently small values of the wavenumber, the vorticity mode is expected to develop a structure similar to that

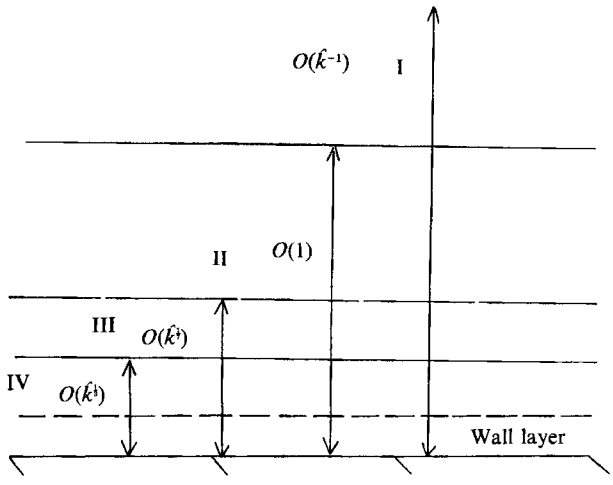

FIGURE 4. The different regions that emerge in the small-$\hat{k}$ limit.

of the 'acoustic' modes. In the following discussion we will isolate the significant asymptotic regimes which occur in the small-wavenumber limit.

The key to understanding the subsequent regimes when $\hat{\alpha}$, $\hat{\beta}$ are related to inverse powers of the Mach number is to write down the small-$\hat{k}$ asymptotic structure of (3.4). Figure 4 is a schematic illustration of the different regions in $\bar{\eta}$-space which, following the analysis of the remainder of this subsection, are found to emerge in the limit $\hat{k} \to 0$. Also shown in this figure is the high-temperature wall layer, $\eta = O(M^{-\frac{1}{2}})$. For the moment $\hat{k}$ is not considered to be sufficiently small for it to be $O(M^{-\check{\phi}})$ for some positive $\check{\phi}$; it then turns out that region II, and to a lesser extent regions I and IV, are passive. However, at sufficiently small values of $\hat{k}$ the wall-layer structure of the basic state will enter the problem – see §3.2. Note that the small-$\hat{k}$ limit to be considered for the remainder of this section corresponds to the 'long-wave' limit considered independently by Grubin & Trigub (1993*b*) for a general Prandtl number, but a power-law type of viscosity.

Careful numerical calculations indicate that $\hat{c}$ becomes large for small values of $\hat{k}$. After some scaling arguments (see §5.1 and/or Blackaby 1991 for details of the type of argument employed) we deduced that $\hat{c}$ expands in the form

$$\hat{c} = \frac{\hat{c}_1}{\hat{k}^{\frac{4}{7}}} + \frac{\hat{c}_2}{\hat{k}^{\frac{3}{7}}} + \frac{\hat{c}_3}{\hat{k}^{\frac{2}{7}}} + \frac{\hat{c}_4}{\hat{k}^{\frac{1}{7}}} + \dots . \tag{3.9}$$

Also, it follows from (2.12*b*), (3.2*b*) and (3.4) that in region I, i.e. for $\bar{\eta} \sim \hat{k}^{-1}$,

$$\hat{p} = \exp(-\hat{k}\bar{\eta}) + \dots,$$

where an arbitrary multiplicative constant has been set equal to one. This solution, together with expansion (3.9), suggest that in region II the pressure should be expanded as

$$\hat{p} = 1 + \hat{k}^{\frac{1}{7}}\hat{p}_1 + \hat{k}^{\frac{2}{7}}\hat{p}_2 + \dots + \hat{k}^{\frac{6}{7}}\hat{p}_6 + \hat{k}(\hat{p}_7 - \bar{\eta}) + \hat{k}^{\frac{8}{7}}(\hat{p}_8 - \hat{p}_1\bar{\eta}) + \hat{k}^{\frac{9}{7}}(\hat{p}_9 - \hat{p}_2\bar{\eta}) + \hat{k}^{\frac{10}{7}}(\hat{p}_{10} - \hat{p}_3\bar{\eta}) + \hat{k}^{\frac{11}{7}}\hat{P}_{11} + \hat{k}^{\frac{12}{7}}\hat{P}_{12} + \hat{k}^{\frac{13}{7}}\hat{P}_{13} + \hat{k}^2\hat{P}_{14} + \dots, \tag{3.10}$$

where we have anticipated the form of several terms in this expansion in that $\hat{p}_1, \hat{p}_2, \dots, \hat{p}_{10}$ are taken as constants, whilst $\hat{P}_{11}$, $\hat{P}_{12}$, etc. are functions of $\bar{\eta}$. At $O(\hat{k}^{\frac{11}{7}})$ we find that $\hat{P}_{11}$ satisfies

$$\hat{P}_{11}'' - 2\bar{G}'/\hat{c}_1 = 0,$$

so that after use of the exponential matching condition it follows that

$$\hat{P}_{11} = -\frac{2}{\hat{c}_1}\int_{\bar{\eta}}^{\infty} \bar{G}\,\mathrm{d}\bar{\eta} - \hat{p}_4\,\bar{\eta} + \hat{p}_{11}, \tag{3.11}$$

where $\hat{p}_{11}$ is another constant. $\hat{P}_{12}$ and $\hat{P}_{13}$ satisfy similar equations with forcing functions coming from the higher-order terms in the expansion of the wave speed.

The $O(\hat{k}^2)$ term in (3.10) is then found to satisfy

$$\hat{P}''_{14} = (1-\bar{G})^2 - \frac{2\bar{G}'}{\hat{c}_1}\left(\hat{p}_3 - \frac{\hat{c}_2}{\hat{c}_1}\hat{p}_2 - \left(\frac{\hat{c}_3}{\hat{c}_1} - \frac{\hat{c}_2}{\hat{c}_1}\right)\hat{p}_1 - \frac{\hat{c}_4}{\hat{c}_1} + \frac{2\hat{c}_2\,\hat{c}_3}{\hat{c}_1^2} - \frac{\hat{c}_2^3}{\hat{c}_1^3}\right),$$

which may be integrated twice to give $\hat{P}_{14}$. However, it is enough for our purposes to note that $\hat{P}_{14} \propto \bar{\eta}^{-6}$ as $\bar{\eta} \to 0$. Hence the $O(\hat{k}^{\frac{11}{7}})$ and $O(\hat{k}^2)$ terms in (3.10) become comparable when $\bar{\eta} = O(\hat{k}^{\frac{1}{7}})$. This suggests that in sublayer III we should define

$$\tilde{\xi} = \hat{k}^{-\frac{1}{7}}\bar{\eta},$$

and expand the pressure as

$$\hat{p} = 1 + \hat{k}^{\frac{1}{7}}\hat{p}_1 + \ldots + \hat{k}\hat{p}_7 + \hat{k}^{\frac{8}{7}}\tilde{P}_8(\tilde{\xi}) + \ldots, \tag{3.12a}$$

where we have, by matching with the solution in II, again anticipated several terms in this expansion. At $O(\hat{k}^{\frac{6}{7}})$ we find that $\tilde{P}_8$ satisfies

$$\tilde{P}''_8 + \frac{72}{\tilde{\xi}(\hat{c}_1\,\tilde{\xi}^4 + 9)}\tilde{P}'_8 = \frac{81}{\tilde{\xi}^8}, \tag{3.12b}$$

with solution

$$\tilde{P}'_8 = \left(\hat{c}_1 + \frac{9}{\tilde{\xi}^4}\right)^2\left(\int_{\infty}^{\tilde{\xi}} \frac{81\,\mathrm{d}\tilde{\xi}}{(\hat{c}_1\,\tilde{\xi}^4 + 9)^2} - \frac{1}{\hat{c}_1^2}\right), \tag{3.12c}$$

where the constant of integration has been chosen to satisfy $\tilde{P}'_8 \to -1$ as $\tilde{\xi} \to \infty$, in order to match with the solution in II. From (3.12*c*), it follows that $\tilde{P}_8 \sim \tilde{\xi}^{-7}$ as $\tilde{\xi} \to 0$, from which it can be easily deduced that (3.12*b*) is no longer the appropriate zeroth approximation to (3.4) when $\bar{\eta} \sim \hat{k}^{\frac{1}{3}}$. This suggests that in sublayer IV we should define $\bar{\eta} = \hat{k}^{\frac{1}{3}}\hat{\xi}$, leading to the zeroth-order approximation to (3.4):

$$\hat{p}_{\hat{\xi}\hat{\xi}\hat{\xi}} + \frac{8}{\hat{\xi}}\hat{p}_{\hat{\xi}\hat{\xi}} - \frac{81}{\hat{\xi}^8}\hat{p}_{\hat{\xi}} = 0. \tag{3.12d}$$

This equation must be solved subject to $\hat{p} \to 0$ as $\hat{\xi} \to 0$. The appropriate solution that matches with the leading term in (3.12*a*) is

$$\hat{p} = \frac{3^{\frac{7}{6}}}{2^{\frac{1}{6}}\Gamma(\frac{7}{6})\,\hat{\xi}^{\frac{7}{2}}}K_{\frac{7}{6}}\left(\frac{3}{\hat{\xi}^3}\right),$$

where $K_{\frac{7}{6}}$ is a modified Bessel function. A complete match with sublayer III can then only be achieved if

$$\int_0^{\infty} \frac{81\,\mathrm{d}\tilde{\xi}}{(\hat{c}_1\,\tilde{\xi}^4 + 9)^2} + \frac{1}{\hat{c}_1^2} = 0. \tag{3.13a}$$

It is assumed in (3.13*a*) that $\hat{c}_1$ is complex; hence the unique root consistent with $\mathrm{Im}\,(\hat{c}_1) > 0$ is

$$\hat{c}_1 = \left(\frac{8\sqrt{2}}{3\sqrt{3\pi}}\right)^{\frac{4}{7}}\exp\left(\frac{4\mathrm{i}\pi}{7}\right), \tag{3.13b}$$

which corresponds to an unstable mode of (2.12a). We note that to leading order the eigenvalue is independent of the Sutherland constant $\check{C}$; indeed all the long-wavelength asymptotes derived below are independent of $\check{C}$ to leading order.

3.2. *Modes with wavelengths comparable with the thickness of the high-temperature region: $\alpha, \beta = O(M^{-\frac{3}{2}})$. The link with acoustic modes*

Next we consider the situation when α, β are so small that region IV in figure 4 merges with the wall layer of the basic state (see §2.1). Since the wall layer is of thickness $M^{-\frac{1}{2}}$, this occurs when $(\alpha, \beta) \sim M^{-\frac{3}{2}}$. It is then appropriate to write

$$(\alpha, \beta) = M^{-\frac{3}{2}}(\alpha_0, \beta_0) + \ldots. \tag{3.14a}$$

Since $(1-c) = O(M^{-\frac{8}{7}})$ from (3.3b) and (3.9), the zero-order approximation to (2.12a) in the wall layer is thus

$$\tilde{p}'' - \frac{2\bar{u}_0'}{\bar{u}_0 - 1}\tilde{p}' - \tfrac{1}{4}(\gamma-1)^2(T_b + \bar{u}_0)^2(1-\bar{u}_0)^2\left((\alpha_0^2+\beta_0^2) - \frac{2\alpha_0^2(1-\bar{u}_0)}{(\gamma-1)(T_b+\bar{u}_0)}\right)\tilde{p} = 0, \tag{3.14b}$$

where a prime denotes a derivative with respect to the wall-layer variable $\xi = M^{\frac{1}{2}}\eta$, and $\bar{u}_0 = f_0'$ is the first term in the expansion of $\bar{u}$ in that layer. The above equation is to be solved subject to $\tilde{p}'(0) = 0$. For large ξ it has the asymptotic solutions

$$\tilde{p} \sim N_0 = \text{constant} \quad \text{and} \quad \tilde{p}\xi^7 \sim N_1 = \text{constant}.$$

For most choices of α_0, β_0, T_b and γ, the constant N_0 is non-zero, and the asymptotic structure for layers I, II, and III survives intact. Thus for these values of α_0 and β_0 the wave speed c expands as (see (3.3), (3.9), (3.13b), (3.14a))

$$c = 1 + \frac{1}{M^{\frac{8}{7}}} \frac{2^{\frac{5}{7}}\hat{c}_1}{(\gamma-1)(T_b+1)(\alpha_0^2+\beta_0^2)^{\frac{2}{7}}} + \ldots, \tag{3.15a}$$

implying that the temporal-wave growth rate, $\mathrm{Im}(\alpha c)$, is of order $M^{-\frac{32}{14}}$. The spatial-wave growth rate is also of this order since the transformation (3.8c), between the temporal and spatial growth rates, is still valid on substitution of the appropriate modified expansion, analogous to (3.15a), for α.

However, equation (3.14b) has a countably infinite set of eigenvalues for which the constant $N_0 = 0$. For two-dimensional disturbances with $T_b = 1$ and $\gamma = 1.4$, a numerical solution of (3.14b) yielded the eigenvalue sequence

$$\alpha_0 = 2.47, 7.17, 12.19, 17.33, 22.54, 27.79, \ldots. \tag{3.15b}$$

The first three eigenfunctions associated with this sequence are shown in figure 5. As explained in the Appendix, the decay of the eigenfunctions away from the wall leads to a dramatic decrease in the growth rate. Moreover, the eigenvalues indicate the existence of neutral acoustic modes that are the counterpart of those discussed by CH for a Chapman-law fluid.

The decrease in growth rate at the discrete set of eigenvalues is reflected in the finite-Mach-number calculations of Mack (1969, 1984, 1987). Mack (1984) numbers each local maximum in growth rate, and identifies the local maxima with different modes. We believe that it is a moot point what these modes are called, e.g. first mode, nth acoustic mode, vorticity mode.† However, what is clear from our analysis is that

† Mack (1987, 1991, private communication) refers to modes where the pressure fluctuation at the wall is larger than that at the generalized inflexion point as acoustic modes, and vice versa for a vorticity mode; other authors have adopted alternative terminology (e.g. SB).

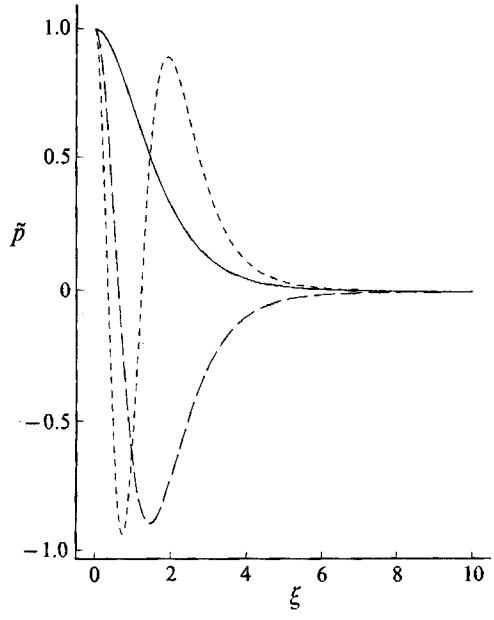

FIGURE 5. The first three neutral acoustic-mode eigenfunctions. Modes 1, 2, 3 have 0, 1, 2 zeros in $(0, \infty)$ respectively.

some of the modes that Mack terms unstable acoustic modes, can, in some asymptotic sense, alternatively be viewed as long-wavelength vorticity modes.

The structure of the modes in the vicinity of the eigenvalues is given in the Appendix. There we show that both inflexional and non-inflexional neutral 'acoustic' modes can be found. However, depending on the parameters of the basic flow, these neutral modes may or may not be the continuation of a long-wavelength vorticity mode (e.g. see also figure 9 of Mack 1987).

We note also that it is possible to seek small-growth-rate acoustic-type modes with $(\alpha, \beta) = O(1)$, i.e. with wavenumbers comparable with those chosen in §3.1. The eigenfunctions for these modes are again concentrated in the $\xi = O(1)$ wall layer, but they now have a fast variation in this layer which can be described using the WKBJ method. At certain values of (α, β) these eigenvalues coalesce with the neutral vorticity mode discussed in §3.1. An analysis outlined in CH, and developed in full in SB, can be performed to describe the 'splitting' of the eigenvalues in this region. We do not pursue this calculation here, since our main concern is with mapping out the full asymptotic structure of the long-wavelength limit of the vorticity mode, e.g. we wish to see if the vorticity mode connects with another neutral state.

Thus the main significance of the $(\alpha, \beta) = O(M^{-\frac{3}{2}})$ asymptotic regime is that it is at this stage that 'acoustic' modes fully emerge. However, apart from asymptotically small regions close to neutral acoustic-mode eigenvalues, the small-wavenumber structure developed initially in §3.1 for $\hat{k} \ll 1$, see (3.3), (3.9), (3.13) and (3.15), survives this regime largely intact. We conclude that the *scaled* departure of the complex wave speed from the unit free-stream velocity increases without bound as the wavenumber decreases to zero, thus suggesting that another asymptotic regime will develop.

3.3. *Modes where the phase and free-stream velocities differ by the order of the sound speed:* $\alpha, \beta = O(M^{-\frac{7}{4}})$

The next significant stage in our description of the long-wavelength limit of the vorticity mode takes place when its phase velocity differs from the free-stream velocity by the order of the sound speed. This occurs when the temperature in the upper layer, i.e. where $\eta \sim \alpha^{-1}$, becomes such that $\bar{T} \sim (\bar{u}-c)^2 M^2$ (see (2.12a)). The pressure eigenfunction in the upper layer then has its decay to zero modified. This situation occurs when

$$c = 1 + \bar{c}_1/M + \ldots, \quad (\alpha, \beta) = (1/M^{\frac{7}{4}})(l, m) + \ldots, \tag{3.16a,b}$$

with the result that the pressure in the upper layer corresponding to region I of figure 4, is given by

$$\tilde{p} \sim \exp\left(-(l^2(1-\bar{c}_1^2)+m^2)^{\frac{1}{2}} M^{-\frac{7}{4}} \eta\right). \tag{3.17}$$

Region II is again passive, while in region III, the disturbance pressure expands as

$$\tilde{p} = 1 + \ldots + \tilde{P}_2(\tilde{\xi})/M^2 + \ldots,$$

where $\tilde{\xi}$ is now defined by $\tilde{\xi} = M^{\frac{1}{4}} \eta$. The perturbation $\tilde{P}_2$ satisfies the equation

$$\tilde{P}_2'' + \frac{288\tilde{B}}{\tilde{\xi}(36\tilde{B} + \bar{c}_1 \tilde{\xi}^4)} \tilde{P}_2' = (l^2+m^2)\left(\frac{36}{\tilde{\xi}^4}\right)^2, \tag{3.18a}$$

where

$$\tilde{B} = \frac{2}{(\gamma-1)(T_b+1)}. \tag{3.18b}$$

The solution of this equation that matches to (3.17) is

$$\tilde{P}_2' = -\left(1 + \frac{36\tilde{B}}{\bar{c}_1 \tilde{\xi}^4}\right)^2 \left(\int_{\tilde{\xi}}^{\infty} \frac{(36\bar{c}_1)^2 (l^2+m^2)}{(36\tilde{B} + \bar{c}_1 \tilde{\xi}^4)^2} \, \mathrm{d}\tilde{\xi} + (l^2(1-\bar{c}_1^2)+m^2)^{\frac{1}{2}}\right). \tag{3.19a}$$

In the wall layer there are now no neutral-acoustic-mode eigenfunctions, and thus the matching condition with (3.17) leads to the eigenrelation

$$\int_0^{\infty} \frac{(36\bar{c}_1)^2 (l^2+m^2)}{(36\tilde{B} + \bar{c}_1 \tilde{\xi}^4)^2} \, \mathrm{d}\tilde{\xi} + (l^2(1-\bar{c}_1^2)+m^2)^{\frac{1}{2}} = 0. \tag{3.19b}$$

A more concise form of (3.19b) is found by writing

$$(l, m) = \frac{8\tilde{B}^{\frac{7}{4}}}{3\sqrt{3\pi}} (\bar{l}, \bar{m}) \tag{3.20a}$$

and then integrating to yield

$$(\bar{l}^2+\bar{m}^2)\,\bar{c}_1^{\frac{7}{2}} + (\bar{l}^2(1-\bar{c}_1^2)+\bar{m}^2)^{\frac{1}{2}} = 0. \tag{3.20b}$$

For large wavenumbers we obtain

$$\bar{c}_1 \sim \frac{\mathrm{e}^{4\mathrm{i}\pi/7}}{(\bar{l}^2+\bar{m}^2)^{\frac{2}{7}}} \quad \text{as} \quad (\bar{l}^2+\bar{m}^2) \to \infty, \tag{3.20c}$$

which matches with (3.13b) and (3.15) as required. For small wavenumbers such that $\bar{m} = O(\bar{l})$, $\bar{l} \ll 1$, we find that

$$\bar{c}_1 \sim \left(\frac{\bar{l}}{\bar{l}^2+\bar{m}^2}\right)^{\frac{4}{3}} \mathrm{e}^{2\mathrm{i}\pi/3}. \tag{3.20d}$$

Further, for two-dimensional modes it is relatively straightforward to show that $(-\bar{c}_{1r})$ and $\bar{c}_{1i}$ are monotonic decreasing functions of $\bar{l}$.

It follows from (3.20*c*, *d*) that for modes with $\bar{m} = O(\bar{l})$ the scaled growth rate, $\mathrm{Im}\,(\bar{l}\bar{c}_1)$, has a local minimum (see also figure 7); similarly the distance from the boundary that the mode is felt, which is inversely proportional to $\bar{l}\bar{c}_1$ (see (3.17)), has a local maximum. We conclude that on the one hand the small (temporal) growth rates seem to diminish the importance of this scaling, while on the other hand its relevance is possibly increased by the fact that the mode extends some distance away from the boundary so making interactions with external flow features such as shocks more likely. Again, as the modes under current consideration are 'near-neutral' (see (3.16*a*)), the spatial growth rates are directly proportional to the temporal growth rates.

Grubin & Trigub (1993*b*) show that the minimum in growth rate is a consequence of our choice of unit Prandtl number. They identify a similarity parameter, s_{gt}, which for a viscosity law proportional to $T^{\frac{1}{2}}$ (i.e. one close to the Sutherland formula), is

$$s_{gt} = \frac{3(2Pr-1)}{Pr+3}.$$

They show that for $0 < s_{gt} < \frac{1}{2}$, a lower-branch neutral mode can be identified on the present scaling, but that for $\frac{1}{2} < s_{gt} < 1$ (the choice $Pr = 1$ yields $s_{gt} = \frac{3}{4}$), there is a minimum in the growth rate (see above).

The increase in the growth rate for small wavenumbers in (3.20*d*) suggests that another asymptotic regime exists for sufficiently long waves. Further, it follows from (3.19*b*) and (3.20*d*) that as $(\bar{l}, \bar{m}) \to 0$ the $M^{-\frac{1}{4}}$ layer decreases in size like $\bar{l}^{\frac{1}{3}}$; as a result, a different asymptotic structure is reached when the $M^{-\frac{1}{4}}$ and $M^{-\frac{1}{2}}$ layers merge for $(\bar{l}, \bar{m}) = O(M^{-\frac{3}{4}})$, $(\alpha, \beta) = O(M^{-\frac{5}{2}})$ and $\bar{c}_1 = O(M)$. This scaling is studied in §3.4.

However, the above is not the only distinguished limit for small wavenumbers; if $\bar{m} = O(\bar{l}^{\frac{7}{11}})$ as $\bar{l} \to 0$, then $\bar{c}_1 = (\bar{l}^{-\frac{4}{11}})$, and the eigenrelation (3.20*b*) simplifies to

$$\bar{m}^2\bar{c}_1^7 + (\bar{m}^2 - \bar{l}^2\bar{c}_1^2)^{\frac{1}{2}} \sim 0. \tag{3.20e}$$

Note that in contrast to modes with comparable wavenumbers, i.e. $\bar{m} = O(\bar{l})$, the growth rate of these strongly oblique modes decreases as $\bar{l}, \bar{m}$ decrease, while the distance the modes extend away from the wall increases. Again, for sufficiently small wavenumbers a new asymptotic regime arises. In particular, because the thickness of the $M^{-\frac{1}{4}}$ layer decreases in size like $\bar{l}^{\frac{11}{11}}$, a rescaling is necessary when $\bar{l} = O(M^{-\frac{11}{4}})$, $\alpha = O(M^{-\frac{9}{2}})$, $\beta = O(M^{-\frac{7}{2}})$, and $c = O(1)$. This scaling is examined in §3.5.

3.4. *Modes with phase velocities comparable with the free-stream velocity:* $\alpha, \beta = O(M^{-\frac{5}{2}})$

Here we expand α, β and c in the forms

$$c = c_0 + \ldots, \quad (\alpha, \beta) = \frac{1}{M^{\frac{5}{2}}}(\hat{l}, \hat{m}) + \ldots. \tag{3.21a}$$

Now there are just three regions, of depth $M^{-\frac{1}{4}}$, M^0, and $M^{\frac{3}{2}}$ to consider. As indicated above, the extent of the perturbation away from the wall has been reduced by a factor of $M^{\frac{1}{4}}$ from the order-$M^{\frac{7}{4}}$ scale in the previous subsection. This reduction in depth arises because the $(\bar{u}-c)$ term in (2.12*a*) is now sufficiently large to dominate the temperature term T. For $H = M^{-\frac{3}{2}}\eta = O(1)$, the leading-order solution to the Rayleigh equation which decays at infinity is

$$\tilde{p} = \exp(-\sigma H), \tag{3.21b}$$

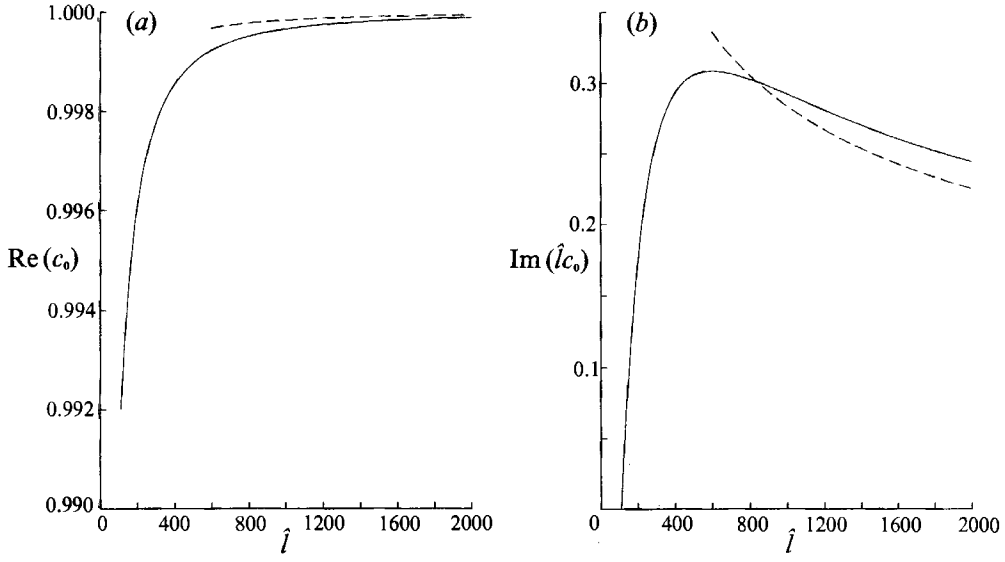

FIGURE 6. (*a*) The real part of the wave speed c_0 as a function of $\hat{l}$ ($\gamma = 1.4$, insulated wall). (*b*) The growth rate $\mathrm{Im}(\hat{l}c_0)$ as a function of $\hat{l}$ ($\gamma = 1.4$, insulated wall).

where $\sigma = \mathrm{i}\hat{l}(1-c_0)$, and it has been assumed that c_0 has a positive imaginary part. Since $\tilde{p}_\eta \to -M^{-\frac{3}{2}}\sigma$ as $H \to 0$, the solution for $\tilde{p}$ in the passive $\eta = O(1)$ region is

$$\tilde{p} = 1 + \ldots + (1/M^{\frac{3}{2}})(\hat{p}_{\frac{3}{2}} - \sigma\eta) + \ldots, \tag{3.21c}$$

where $\hat{p}_{\frac{3}{2}}$ is a constant and, as before, the dots indicate other constant terms which can be found by matching. It remains to consider the high-temperature layer where $\eta = M^{-\frac{1}{2}}\xi$. Here $\tilde{p}$ expands as

$$\tilde{p} = 1 + \ldots + (1/M^2)\bar{P}_2(\xi) + \ldots, \tag{3.22a}$$

which leads to the governing equation for $\bar{P}_2$:

$$\bar{P}_2'' - \frac{2u_0'}{u_0 - c_0}\bar{P}_2' = \tfrac{1}{4}(\hat{l}^2 + \hat{m}^2)(\gamma-1)^2(T_b + u_0)^2(1-u_0)^2 - \tfrac{1}{2}\hat{l}^2(\gamma-1)(T_b+u_0)(1-u_0)(u_0-c_0)^2. \tag{3.22b}$$

A solution can be found which satisfies both the boundary condition on $\xi = 0$ and the matching condition with (3.21*c*), if

$$(1-c_0)\int_0^\infty \frac{(\gamma-1)(T_b+u_0)(1-u_0)}{4(u_0-c_0)^2}((\hat{l}^2+\hat{m}^2)(\gamma-1)(T_b+u_0)(1-u_0) - 2\hat{l}^2(u_0-c_0)^2)\,\mathrm{d}\xi = -\mathrm{i}\hat{l}. \tag{3.23}$$

This is the required eigenrelation to determine the complex wave speed c_0 as a function of the scaled wavenumbers $\hat{l}, \hat{m}$. A large-wavenumber analysis of this equation shows that the eigenvalue matches to (3.20*d*).

In figure 6 we show the wave speed and growth rate as a function of $\hat{l}$ for a two-dimensional mode in the case of an insulated wall. The maximum value of $\mathrm{Im}(\hat{l}c_0)$ occurs for $\hat{l} \sim 598$, and a neutral mode exists for $\hat{l} \sim 111$; the neutral mode takes the form of a radiating sound wave far from the boundary. It follows that two-

dimensional modes do not exist for sufficiently small wavenumbers, although three-dimensional modes with small wavenumbers can be found. In particular, if $\hat{l} \to 0$ such that

$$\hat{m} = \hat{r}\hat{l}^{\frac{1}{2}}, \tag{3.24a}$$

where $\hat{r} = O(1)$, then to leading order (3.23) reduces to

$$\hat{r}^2(1-c_0)\int_0^\infty \frac{(\gamma-1)^2(T_b+u_0)^2(1-u_0)^2}{4(u_0-c_0)^2}\,\mathrm{d}\xi = -\mathrm{i}. \tag{3.24b}$$

For an insulated wall, growing modes can be found for $\hat{r} \geqslant 3.2$, and hence for sufficiently oblique modes there is no small-wavenumber cutoff on this scale. At very small wavenumbers these oblique three-dimensional waves match onto modes with $\alpha = O(M^{-\frac{9}{2}})$, $\beta = O(M^{-\frac{7}{2}})$ – see §3.5. Note that since the wave speed now differs by an order-one amount from the free-stream speed (see (3.21*a*)), the spatial instability properties cannot be immediately deduced from the temporal ones. However, (3.23) is still the leading-order dispersion relation.

To summarize the results for this scaling: (*a*) a lower branch neutral curve for 'moderately' oblique modes can be found, (*b*) for fixed spanwise wavenumbers there is a local maximum in the growth rate as the streamwise wavenumber varies, and (*c*) the most unstable temporal mode for this scaling is two-dimensional.

3.5. *Highly oblique long-wavelength modes:* $\alpha = O(M^{-\frac{9}{2}})$, $\beta = O(M^{-\frac{7}{2}})$, $c = O(1)$

The analysis for this scaling proceeds much as in the previous two subsections. We write

$$c = c_0 + \ldots, \quad (\alpha, \beta) = (\check{l}/M^{\frac{9}{2}}, \check{m}/M^{\frac{7}{2}}) + \ldots, \tag{3.25}$$

then in the outer layer where $\eta = O(M^{\frac{7}{2}})$,

$$\tilde{p} \sim \exp(-\sigma M^{-\frac{7}{2}}\eta), \tag{3.26a}$$

with

$$\sigma = \mathrm{i}(\check{l}^2(1-c_0)^2 - \check{m}^2)^{\frac{1}{2}}, \quad \text{and} \quad \mathrm{Re}(\sigma) > 0. \tag{3.26b}$$

The middle layer, defined as where $\eta = O(1)$, is again passive (cf. (3.21*c*)), while in the high-temperature boundary layer we write

$$\tilde{p} = 1 + \ldots + (1/M^4)\check{P}_4(\xi) + \ldots. \tag{3.27a}$$

The governing equation of $\check{P}_4$ has a solution that both satisfies the boundary condition at the wall and matches with (3.26), if

$$\check{m}^2(1-c_0)^2\int_0^\infty \frac{(\gamma-1)^2(T_b+u_0)^2(1-u_0)^2}{4(u_0-c_0)^2}\,\mathrm{d}\xi = -\mathrm{i}(\check{l}^2(1-c_0)^2 - \check{m}^2)^{\frac{1}{2}}. \tag{3.27b}$$

As $\check{l}, \check{m} \to \infty$, this expression can be shown to match with (3.20*e*) and (3.24*b*) if $\check{m} = O(\check{l}^{\frac{7}{11}})$ and $\check{m} = O(\check{l}^{\frac{1}{2}})$ respectively. As $\check{l}, \check{m} \to 0$, the growth rate of the mode decreases, and for $\check{l} < \check{m} \ll 1$ an asymptotic expansion of (3.27*b*) shows that $c_0 = O(\check{m})$, while $\mathrm{Im}(c_0) = O(\check{m}^2)$. This behaviour is analogous to that at small wavenumbers for instability modes of the incompressible Rayleigh equation. Further, a scaling argument shows that viscous effects are no longer negligible when

$$(\alpha, \beta/M) = O(R^{-\frac{1}{12}}M^{-\frac{15}{4}}). \tag{3.28}$$

Except for the factors of M, this is essentially the viscous scaling for neutral, 'upper-branch', Tollmien–Schlichting waves in slightly compressible flow (e.g. Gajjar & Cole 1989). For hypersonic flow a neutral mode does not exist on this scaling. However,

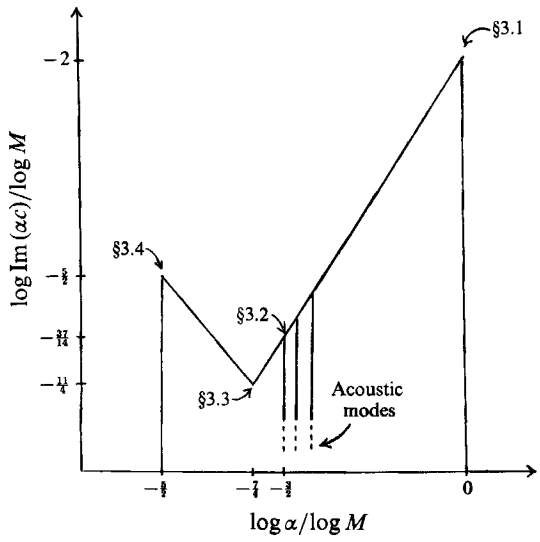

FIGURE 7. Schematic illustration of the growth rate of two-dimensional modes for different wavelengths. There are an infinite number of neutral acoustic modes. In the neighbourhood of these modes typical growth rates are $O(M^{-5})$.

a small-wavenumber expansion based on the scaling (3.28) can be shown to match with the lower-branch, triple-deck, Tollmien–Schlichting waves studied by Smith (1989) and CH.

This completes our asymptotic description of quasi-parallel instability modes of basic flows far downstream of any leading-edge for unit Prandtl number. The major asymptotic regimes of inviscid modes have been identified, and we have indicated how inviscid modes can be matched to highly oblique Tollmien–Schlichting waves. A schematic indicating the temporal growth-rate for different wavenumbers is given in figure 7 for two-dimensional modes.

We have found that: (*a*) the fastest growing modes have $(\alpha, \beta) = O(1)$ and $\mathrm{Im}\,(\omega) = O(M^{-2})$, (*b*) the two-dimensional modes whose influence extends furthest from the boundary have $\alpha = O(M^{-\frac{7}{4}})$, $\mathrm{Im}\,(\omega) = O(M^{-\frac{11}{4}})$ and an $O(M^{\frac{7}{4}})$ scale normal to the boundary, and (*c*) the modes whose influence is felt furthest from the boundary are the three-dimensional, highly oblique, lower-branch Tollmien–Schlichting waves studied by Dunn & Lin (1955), Ryzhov (1984), Smith (1989) and CH.

Finally, if non-parallel effects are to be negligible we require

$$\alpha \gg R^{-\frac{1}{8}}. \tag{3.29}$$

For example, in the case of the longest waves that we have studied in detail, i.e. those with scaling (3.25), this criterion is $R \gg M^9$; this condition is also that for non-parallel effects to be negligible in the case of lower-branch Tollmien–Schlichting waves (Blackaby 1991 – see also Smith 1989).

4. The inviscid instability problem in interactive boundary layers

We consider now the hypersonic flow of a Sutherland-formula fluid past an aligned semi-infinite flat plate when leading-edge effects cannot be neglected. We assume that the plate has a sharp leading edge. There will then be an attached shock which acts as an upper boundary for disturbances. The steady flow beneath the shock has

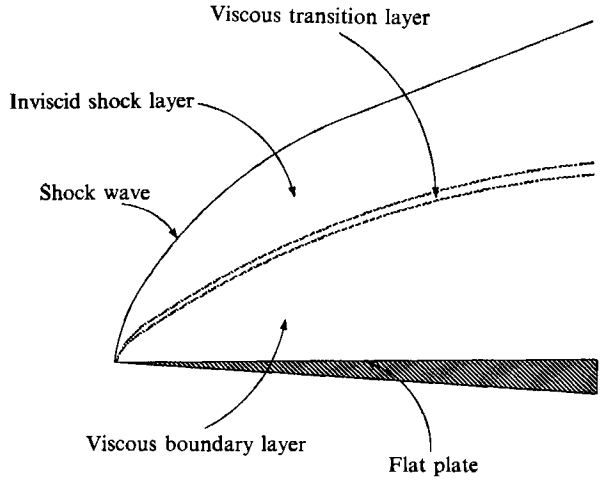

FIGURE 8. The different parts of the flow field in the hypersonic limit.

been studied by Stewartson (1955, 1964), Bush (1966) and others. Our formulation closely follows this earlier work, and so the reader is referred there for a detailed formulation. Only the parts of the solution that we require are outlined below.

As before a choice of viscosity law must be made. Mathematical simplifications sometimes arise with the choice of the model Chapman law. However, in interactive *hypersonic* flow no significant complications arise from the use of Sutherland's formula – primarily because the viscous layers are regions of high temperature where Sutherland's formula reduces to a power law, $\mu \propto T^{\breve{\sigma}}$, with $\breve{\sigma} = \frac{1}{2}$. The steady hypersonic flow of a general power-law fluid past a flat plate has been studied by Luniev (1959) and Bush (1966) among others.

Figure 8 illustrates the distinct asymptotic regions that describe the different parts of the flow field beneath the shock. The lower region is hot and viscous, and of comparable thickness to the cooler, inviscid, upper region. Between these two layers is a thin viscous adjustment region, whose accurate description is vital to the correct formulation of the instability problem. We consider each of these regions in turn.

4.1. *The upper inviscid region*

Since viscosity is negligible in this region, the choice of viscosity law does not alter the well-known governing equations. As in previous studies we assume that the steady flow is two-dimensional, and introduce the steady streamfunction ψ defined by

$$\rho u = \psi_y, \quad \rho v = -\psi_x. \tag{4.1a,b}$$

Then the velocity, temperature, density and pressure are expanded as

$$(u-1, v, T, \rho, p) = (u_1/M^2, v_1/M, T_1, \rho_1, p_1/M^2) + \ldots. \tag{4.2a–e}$$

On substituting into (2.2) and (2.3), and re-writing the equations in terms of Von-Mises coordinates using the scaled streamfunction

$$\tilde{\psi} = M\psi, \tag{4.2f}$$

the leading-order governing equations are found to be

$$v_{1x} = -p_{1\tilde{\psi}}, \quad v_{1\tilde{\psi}} = (\partial/\partial x)\,(1/\rho_1), \quad p_1 = E(\tilde{\psi})\,\rho_1^{\gamma}. \tag{4.3a–c}$$

The function $E(\tilde{\psi})$ can, in principle, be evaluated from the initial conditions for these hyperbolic equations. The latter are specified at the shock, which is taken to be at $y = M^{-1}F(x)$, for some unknown function F. Conservation of mass, and the Rankine–Hugoniot relations imply that at the shock

$$\tilde{\psi} = F, \quad v_1 = \frac{2(F'^2-1)}{(\gamma+1)F'}, \quad p_1 = \frac{(2\gamma F'^2-\gamma+1)}{\gamma(\gamma+1)}, \quad \rho_1 = \frac{(\gamma+1)F'^2}{2+(\gamma-1)F'^2}. \tag{4.4a–d}$$

4.2. *The strong-interaction zone*

The solution of (4.3), (4.4), and the corresponding equations for the lower layers, can be investigated analytically for large and small x using expansion procedures, e.g. Stewartson (1955, 1964), Bush (1966), Bush & Cross (1967), Brown & Stewartson (1975). We will concentrate on the small-x solution valid very close to the leading edge of the plate, although equivalent expressions for large x can be found.

Since the shock is attached to the leading edge, for $x \ll 1$ it follows that $F \propto x^n$. Then a scaling argument based on (4.3) and (4.4), together with the viscous equations (4.10), (4.11) and (4.12) given below, shows that the pressure and normal velocity in the different asymptotic regions match if $n = \frac{3}{4}$ (e.g. Stewartson 1964; Bush 1966). The appropriate similarity solution is thus of the form:

$$F = a_1 x^{\frac{3}{4}} + \ldots, \quad \tilde{\psi} = a_1 x^{\frac{3}{4}} \bar{\psi}, \tag{4.5a, b}$$

$$v_1 = a_1 x^{-\frac{1}{4}} \bar{v}_1(\bar{\psi}) + \ldots, \quad p_1 = a_1^2 x^{-\frac{1}{2}} \bar{p}_1(\bar{\psi}) + \ldots, \quad \rho_1 = \bar{\rho}_1(\bar{\psi}) + \ldots. \tag{4.5c–e}$$

On substitution of (4.5) into (4.3) and (4.4), it follows that

$$E(\tilde{\psi}) \sim e_1 a_1^{\frac{8}{3}} \tilde{\psi}^{-\frac{2}{3}} \quad \text{as} \quad \tilde{\psi} \to 0, \quad \text{where} \quad e_1 = \frac{9(\gamma-1)^\gamma}{8(\gamma+1)^{\gamma+1}}, \tag{4.6a, b}$$

and that

$$\bar{v}_1 + 3\bar{\psi}\bar{v}_1' = 4\bar{p}_1', \quad \bar{p}_1(\bar{\psi}) = \frac{e_1}{\bar{\psi}^{\frac{2}{3}}} \bar{\rho}_1^\gamma(\bar{\psi}), \quad \bar{v}_1' = \frac{3\bar{\psi}}{4\bar{\rho}_1^2} \bar{\rho}_1', \tag{4.7a–c}$$

where

$$\bar{v}_1 = \frac{3}{2(\gamma+1)}, \quad \bar{p}_1 = \frac{9}{8(\gamma+1)}, \quad \bar{\rho}_1 = \frac{\gamma+1}{\gamma-1} \quad \text{on} \quad \bar{\psi} = 1. \tag{4.7d–f}$$

For given γ a numerical solution can be found for $\bar{\psi} < 1$; in particular $\bar{p}_{10} \equiv \bar{p}_1(0)$ and $\bar{v}_{10} \equiv \bar{v}_1(0)$ can be evaluated. Note that $\bar{\rho}_1 \propto \bar{\psi}^{\frac{2}{3\gamma}}$ as $\bar{\psi} \to 0$, and thus we require $\gamma > \frac{2}{3}$ if the leading-order solution for v_1 is to have the form (4.5c); this condition is satisfied for a realistic gas.

The no-slip boundary condition is not satisfied by (4.2a), and thus there is at least one viscous sublayer beneath the present region. We consider next the viscous boundary layer which is immediately adjacent to the surface of the plate.

4.3. *The viscous boundary layer*

As is conventional the pressure does not vary significantly across this boundary layer, and it is appropriate to take $T = O(M^2)$ as in §2. It follows from (2.2d), (4.1b) and (4.2e) that $\psi = O(M^{-3})$, and so we introduce the scaled streamfunction

$$\Psi = M^3 \psi. \tag{4.8}$$

A balance between viscous and inertia forces then demonstrates that the hypersonic parameter, r, defined by

$$R = rM^5, \tag{4.9}$$

should be taken to be order one (Luniev 1959). (Note that by a suitable redefinition of the lengthscale L we could take $r = 1$ without loss of generality.) Recall that the power of the Mach number is six in the definition of the hypersonic parameter for a linear viscosity law. The appropriate expansions of the flow quantities are

$$(u, v, p, \rho, T, \mu) = \left(U_1, \frac{1}{M}V_1, \frac{1}{M^2}P_1, \frac{1}{M^2}R_1, M^2\theta_1, M\mu_1\right) + \ldots, \tag{4.10a–f}$$

with $\mu_1 = (1+\check{C})\,\theta_1^{\frac{1}{2}}$.

In order to simplify the analysis, we now assume that the wall is an insulator. As we are once again taking the Prandtl number to be unity, the energy equation can then be integrated once to obtain (but see Stewartson 1964, for a caveat)

$$\theta_1 = \tfrac{1}{2}(\gamma-1)\,(1-U_1^2). \tag{4.11}$$

We do not expect the relaxation of these assumptions to substantially alter our main conclusions, but they allow us to explain more simply the effect of the shock on the inviscid modes.

The streamfunction is again adopted as an independent variable instead of y. The x-momentum equation in the boundary layers then becomes

$$U_1 U_{1x} = -\frac{(\gamma-1)}{2}\frac{(1-U_1^2)}{\gamma P_1}P_{1x} + \frac{\gamma P_1 U_1}{r}\left(\frac{\mu_1}{\theta_1}U_1 U_{1\Psi}\right)_\Psi, \tag{4.12}$$

where $P_1 \equiv P_1(x) = p_1(x,0)$. The boundary conditions on the wall, and the matching conditions with the upper inviscid layer, yield

$$U_1 = 0 \quad \text{on} \quad \Psi = 0, \qquad U_1 \to 1 + O(\Psi^{-4}) \quad \text{as} \quad \Psi \to \infty, \tag{4.13a,b}$$

and after some manipulation

$$v_1(x,0) = \left(\frac{\gamma-1}{2\gamma}\right)\frac{\partial}{\partial x}\left(\int_0^\infty \frac{1-U_1^2}{P_1 U_1}\,\mathrm{d}\Psi\right), \tag{4.14}$$

where we have anticipated the fact that the viscous adjustment region plays a passive role as far as leading-order matching is concerned.

4.4. *The boundary-layer solution in the strong-interaction zone*

For small x we introduce the similarity variable $\bar{\Psi}$, and the velocity function $\bar{U}(\bar{\Psi})$, defined by

$$\Psi = (4\gamma(1+\check{C})\,\bar{p}_{10})^{\frac{1}{2}}\left(\frac{2}{\gamma-1}\right)^{\frac{1}{4}}\frac{a_1 x^{\frac{1}{4}}}{r^{\frac{1}{2}}}\bar{\Psi}, \quad U_1 = \bar{U}(\bar{\Psi}) + \ldots \tag{4.15a,b}$$

(see Lees 1953). The boundary-layer equation (4.12) then takes the similarity form

$$-\bar{\Psi}\bar{U}\bar{U}' = \left(\frac{\gamma-1}{\gamma}\right)(1-\bar{U}^2) + \bar{U}\left(\frac{\bar{U}\bar{U}'}{(1-\bar{U}^2)^{\frac{1}{2}}}\right)', \tag{4.16}$$

with boundary conditions

$$\bar{U}(0) = 0, \quad \bar{U} = 1 - \frac{18\gamma^2}{(3\gamma-1)^2\bar{\Psi}^4} + \ldots \quad \text{as} \quad \bar{\Psi} \to \infty. \tag{4.17a,b}$$

This is a modified Falkner–Skan equation where $\bar{U}$ decays algebraically rather than exponentially for large $\bar{\Psi}$. Substitution of (4.15) into (4.12) and use of (4.5) yields the leading-order coefficient a_1 in the small-x expansion for the as yet unknown shock location:

$$a_1^2 = \frac{3(1+\check{C})^{\frac{1}{2}}}{4\bar{v}_{10}}\left(\frac{2(\gamma-1)}{r\gamma\bar{p}_{10}}\right)^{\frac{1}{2}}\left(\frac{\gamma-1}{2}\right)^{\frac{1}{4}}\int_0^\infty \frac{1-\bar{U}^2}{\bar{U}}\,\mathrm{d}\Psi. \tag{4.18}$$

The value $a_1^2 = 2.7842533$ was obtained numerically for our chosen parameter values: $\check{C} = 0.509$, $\gamma = 1.4$, $r = 1$.

4.5. *The viscous adjustment layer*

The existence of this layer can be seen by considering the limiting forms of the temperature at the edges of the upper and lower layers. First, from (2.2*d*), (4.2), (4.3*c*) and (4.6) it follows that

$$T \sim T_1 \sim \gamma p_1(x,0)^{\frac{\gamma-1}{\gamma}}(e_1^3 a_1^8/\tilde{\psi}^2)^{\frac{1}{3\gamma}} \quad \text{as} \quad \tilde{\psi}\to 0. \tag{4.19}$$

Second, as the top edge of the boundary layer is approached from below we see from (4.8), (4.10*e*), (4.11) and (4.13*b*) that

$$T = M^2\theta_1 \propto M^2/\Psi^4 \propto 1/(M^6\tilde{\psi}^4) \quad \text{as} \quad \Psi\to\infty. \tag{4.20}$$

Since (4.19) and (4.20) do not match, there must be an intermediate asymptotic region (cf. the temperature adjustment region of §2.2); this occurs where the scaled streamfunction, ζ, defined by

$$\zeta = \tilde{\psi}M^\lambda = \psi M^{\lambda+1}, \quad \text{with} \quad \lambda = 9\gamma/(6\gamma-1), \tag{4.21a,b}$$

is order one. Unfortunately, because the power of M is a function of γ, some of the following expansions are algebraically complicated.

Examination of the small-$\tilde{\psi}$ limit of the inviscid solution implies that the appropriate expansions in the adjustment layer are

$$(u-1, v, T, p, \rho) = \left(\frac{1}{M^{\frac{12\gamma-6}{6\gamma-1}}}\tilde{U}_1, \frac{1}{M}v_1(x,0), M^{\frac{6}{6\gamma-1}}\tilde{T}_1, \frac{1}{M^2}P_1, \frac{1}{M^{\frac{6}{6\gamma-1}}}\frac{\gamma P_1}{\tilde{T}_1}\right)+\ldots, \tag{4.22a–e}$$

where we have anticipated the fact that the leading-order contributions to v and p are independent of ζ, and can hence be fixed by matching. When these expansions are substituted into the Navier–Stokes equations, and the energy equation is integrated once, we obtain in terms of Von-Mises coordinates

$$\tilde{U}_{1x} = -\frac{\tilde{T}_1 P_{1x}}{\gamma P_1} + \frac{\gamma(1+\check{C})P_1}{r}\frac{\partial}{\partial\zeta}\left(\frac{1}{\tilde{T}_1^{\frac{1}{2}}}\frac{\partial\tilde{U}_1}{\partial\zeta}\right), \tag{4.23}$$

$$\tilde{T}_1 = (1-\gamma)\tilde{U}_1. \tag{4.24}$$

Equation (4.23) is a perturbation form of (4.12), and hence in this adjustment layer the high-temperature form of Sutherland's formula is still valid. This is in contrast with the shock-free adjustment layer where the full form occurred – see (2.10*a*).

Again, a similarity form of these equations can be found for $x \ll 1$. Using (4.5*d*), (4.15), (4.17*b*), (4.19) and (4.20) it follows that the appropriate similarity variable is s, defined by

$$s = x^{(\lambda-3)/4}\zeta/b_1, \quad \text{where} \quad b_1^2 = (1+\check{C})\gamma a_1^2\bar{p}_{10}/r. \tag{4.25a,b}$$

This is in agreement with Bush's (1966) result. Writing

$$\tilde{U}_1 = x^{\lambda-2} G(s), \tag{4.26a}$$

and using (4.5*d*), we find that the governing equation for the flow solution in this crucial region is

$$(\lambda-2)\,G - \frac{3-\lambda}{4} sG' = \frac{1-\gamma}{2\gamma} G + \left(\frac{G'}{[(1-\gamma)\,G]^{\frac{1}{2}}}\right)'. \tag{4.26b}$$

From (4.22*a*) and (4.26*a*), we expect that $G < 0$.

As $s \to 0$ we find that G has the asymptotic behaviour

$$G = -G_0 s^{-4} + G_1 s^{-q} + \ldots, \quad \text{where} \quad G_0 = \frac{576\gamma^2}{(\gamma-1)(3\gamma-1)^2}. \tag{4.27a,b}$$

Thus the adjustment-layer solution matches onto the large-$\bar{Y}$ form of $\bar{U}$. The coefficient G_1 must be determined from a numerical solution of (4.26*b*), but the parameter q satisfies a quadratic equation with coefficients that are functions of γ (in fact $q < 1$ if $\gamma > \frac{2}{3}$). This quadratic equation, as well as the above expression for G_0, is obtained by substituting (4.27*a*) into (4.26*b*) and then equating coefficients of the first two leading inverse powers of s. With $\gamma = 1.4$ we find that $G_0 \approx 275.6$ and $q \approx 0.6267$, so that the correction terms are relatively small.

For large s we find that

$$G \to -A_0 s^{-\frac{2}{3\gamma}} - \frac{8A_0^{\frac{1}{2}}(3\gamma+1)}{9\gamma(\gamma-1)^{\frac{1}{2}}(3\gamma-1)} s^{-2-\frac{1}{3\gamma}} + \ldots, \tag{4.28}$$

where from matching with the inviscid solution in the upper layer,

$$A_0 = \frac{a_1^2}{\gamma-1}\left(\frac{\gamma^{3\gamma-1} r \bar{p}_{10}^{3\gamma-4} e_1^3}{(1+\check{C})}\right)^{\frac{1}{3\gamma}}. \tag{4.29}$$

For the choices $r = 1$, $\gamma = 1.4$ and $\check{C} = 0.509$, we find $A_0 \approx 0.744\,528\,16$. Note that G decays algebraically for large s, in contrast to the rapid exponential decay of both the Blasius function and the 'Modified Blasius' function (2.10*c*), which arise in the shock-free, far-downstream cases (the former after employing Chapman's law, and the latter from the use of the more realistic Sutherland's formula).

Now that the leading-order base flow for this region has been identified, we can consider its stability characteristics. In particular we are interested in the linear stability of inviscid modes concentrated (trapped) within this adjustment layer.

4.6. *The vorticity mode in the strong-interaction zone*

The scalings for these modes appear complicated but follow in a straightforward manner after applying the usual vorticity-mode arguments to the flow field discussed above. In particular, we require that the modes should have wavelengths comparable with the physical thickness of the adjustment region, because that is where the generalized inflexion point occurs. A Rayleigh-style analysis using the streamfunction as normal coordinate, rather than the related Dorodnitsyn–Howarth variable, suggests that we require $\partial_{\psi\psi} \sim T^2\check{\alpha}^2$, where $\check{\alpha}$ is the streamwise wavenumber non-dimensionalized using L. From (4.21) and (4.22*c*) we have $T \sim M^{4\lambda-6}$ and $\psi \sim M^{-\lambda-1}$. We deduce that $\check{\alpha} \sim M^{7-3\lambda} \gg 1$, which indicates that this is a short-wavelength mode. The timescale can be deduced by using the fact that vorticity

modes propagate in a frame moving with a velocity approximately equal to that of the fluid in the adjustment layer – see (4.22a). The appropriate 'fast' space and timescales which describe the dynamics of the instability are thus

$$X = M^{7-3\lambda}(x-t), \quad Z = M^{7-3\lambda}z, \quad \tau = M^{\lambda-1}t. \tag{4.30a–c}$$

Since we wish to allow for the possibility that non-parallel effects are important, scaling (4.30) leads to the leading-order multiple-scales transformations

$$\partial_x \to \partial_x + M^{7-3\lambda}\partial_X, \quad \partial_z \to M^{7-3\lambda}\partial_Z, \quad \partial_t \to M^{\lambda-1}\partial_\tau - M^{7-3\lambda}\partial_X. \tag{4.31a–c}$$

Non-parallel effects are $O(\partial_x) \sim O(1)$, and are thus of higher order in comparison with the direct growth effects of magnitude $\check{\alpha}(u-1) = O(M^{\lambda-1}) \gg 1$ ($\lambda = 1.7027$ for our choice of $\gamma = 1.4$). To be consistent with (4.30) and (4.31) we require that $(c-1) = O(u-1)$, and thus the wave speed is expanded as

$$c = 1 + \hat{c}/M^{4(2-\lambda)} + \ldots. \tag{4.32}$$

Now that the scales have been deduced, the remainder of the analysis follows the classical inviscid-mode approach for formulating the pressure equation describing linear wave-like disturbances. We perform a normal-mode analysis, and assume that the infinitesimal pressure disturbance, $\tilde{p}$, is such that

$$\tilde{p} \propto \mathrm{e}^{\mathrm{i}(\alpha X + \beta Z - \alpha\hat{c}\tau)}, \tag{4.33a}$$

where for algebraic simplicity we have redefined the wavenumbers α and β in comparison with (2.11). Estimates similar to those above show that in the adjustment layer the scales for the perturbation velocities, temperature and density are

$$(\tilde{u}, \tilde{v}, \tilde{w}) = O(M^2\tilde{p}), \quad \tilde{T} = O(M^4\tilde{p}), \quad \tilde{\rho} = O(M^{16-8\lambda}\tilde{p}). \tag{4.33b}$$

After substituting these perturbations into a linearized version of the full equations (2.2), and assuming that $\gamma < \frac{8}{3}$, some lengthy manipulation yields a simplified Rayleigh equation for the amplitude of the disturbance pressure, $\hat{p} \equiv \hat{p}(x, \zeta)$:

$$\hat{p}_{\zeta\zeta} - \frac{2\tilde{U}_{1\zeta}(x,\zeta)}{\tilde{U}_1(x,\zeta) - \hat{c}(x)}\hat{p}_\zeta - \frac{(\gamma-1)^2\tilde{U}_1^2(x,\zeta)}{\gamma^2 P_1^2(x)}k^2(x)\,\hat{p} = 0, \tag{4.34}$$

where $k^2 = \alpha^2 + \beta^2$, and $\hat{p}$ decays to zero for large and small ζ. This equation, which describes short-wavelength vorticity modes at any location x in the interaction zone, could have been immediately deduced from the compressible version of Rayleigh's equation; however, without the lengthy substitution performed above there would have been no guarantee that it was an asymptotic approximation. Rather than compute numerical solutions of $\tilde{U}_1$ for $x = O(1)$, we again chose to consider the strong-interaction limit $x \ll 1$.

From (4.5d), (4.25) and (4.26a) the appropriate small-x dependences for $\hat{c}$ and k are

$$\hat{c} = x^{\lambda-2}\mathscr{C}, \quad k = \frac{\gamma a_1^2 \bar{p}_{10}}{b_1(\gamma-1)\,x^{3(\lambda-1)/4}}\mathscr{K}. \tag{4.35a, b}$$

These lead to the following vorticity-mode equation for the pressure in the strong-interaction zone (cf. (3.4a)):

$$\hat{p}_{ss} - \frac{2G'}{G-\mathscr{C}}\hat{p}_s - \mathscr{K}^2G^2\hat{p} = 0. \tag{4.36}$$

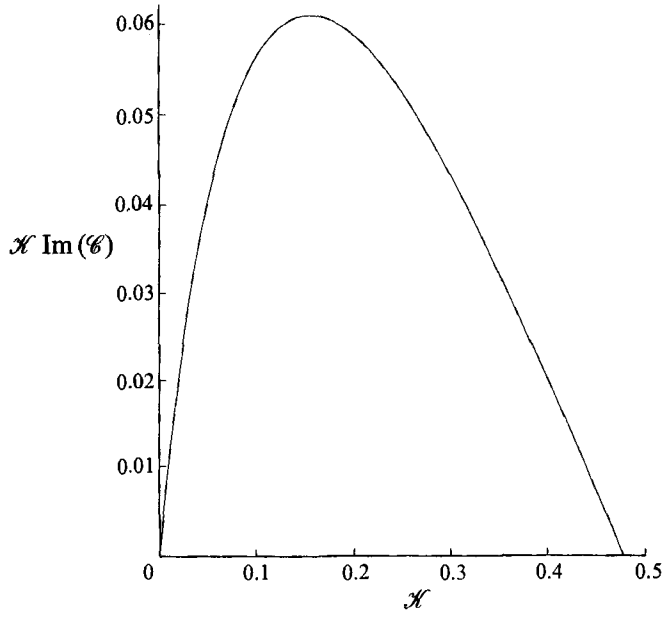

FIGURE 9. The growth rate, $\mathscr{K}$ Im ($\mathscr{C}$), of the vorticity mode in the strong-interaction region as a function of the wavenumber $\mathscr{K}$.

This is to be solved subject to $\hat{p} \equiv \hat{p}(s)$ vanishing in the limits $s \to 0$ and $s \to \infty$, so that the disturbance is again confined to the adjustment layer. The leading-order asymptotes are found to be

$$\hat{p} \to \hat{p}_0 s^{-2} \exp\left(-\frac{G_0 \mathscr{K}}{3s^3}\right) \quad \text{as} \quad s \to 0, \tag{4.37a}$$

$$\hat{p} \to \hat{p}_\infty s^{\frac{1}{3\gamma}} \exp\left(-\frac{3\gamma A_0}{3\gamma - 2} \mathscr{K} s^{\frac{3\gamma-2}{3\gamma}}\right) \quad \text{as} \quad s \to \infty, \tag{4.37b}$$

where $\hat{p}_0$ and $\hat{p}_\infty$ are constants. Higher-order terms in these expressions can be found analytically, and are needed for accurate numerical solutions. We discuss our numerical results, and the asymptotic solution for small wavenumber, in the next section. However, we note from (4.35) that

$$k\hat{c} \propto x^{(\lambda-5)/4} = x^{\frac{5-21\gamma}{4(6\gamma-1)}} \to \infty \quad \text{as} \quad x \to 0.$$

Hence, the fastest growing modes occur infinitely close to the leading edge of this scale. Of course, in practice it may not be feasible to excite such short-wavelength, high-frequency waves.

5. The solution of the strong-interaction vorticity-mode equation

First we consider the upper-branch neutral mode; $\mathscr{C}$ is then real and equal to G evaluated at the generalized inflexion point where

$$GG_{ss} = 2G_s^2. \tag{5.1}$$

A numerical solution to (4.26*b*) using a Runge–Kutta method shows that for $\gamma = 1.4$ this occurs when $\hat{s} \approx 1.661432$, where the new variable $\hat{s} = \ln s$ was

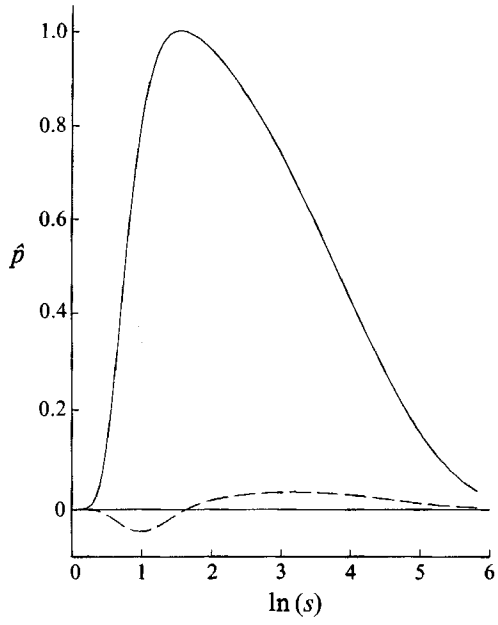

FIGURE 10. The complex eigenfunction of the most dangerous mode in the strong-interaction limit. The solid line corresponds to the real part for the normalization chosen here.

introduced to stretch the coordinate in the small-s region where G and $\hat{p}$ vary rapidly. The resulting neutral wave speed is given by $\mathscr{C} \approx -0.633318$. The corresponding real wavenumber $\mathscr{K}$ is obtained from a numerical solution of (4.36) using a method similar to that outlined in §3.1. The neutral wavenumber was calculated to be $\mathscr{K} \approx 0.477957$. These numerical results are for $\gamma = 1.4$; note that G, and hence solutions to (4.36), need to be re-computed for each choice of γ.

The strong-interaction vorticity-mode equation (4.36) was also solved using a Runge–Kutta method; for a fixed, real value of $\mathscr{K}$, we iterated on the value of complex $\mathscr{C}$ until the boundary conditions (4.37) were satisfied. Figure 9 shows the (temporal) growth rate for two-dimensional waves, Im $(\mathscr{K}\mathscr{C})$, plotted against $\mathscr{K}$ for $\gamma = 1.4$, $\tilde{C} = 0.509$, $r = 1$. Observe that the maximum (temporal) growth rate, Im $(\mathscr{K}\mathscr{C}) \approx 0.060918$, occurs at $\mathscr{K} \approx 0.156100$, and that the growth rate goes to zero as the wavenumber goes to zero. Figure 10 illustrates the complex eigenfunction of the most unstable mode, including the exponential decay of the eigenfunction at both ends of the range of integration. The spatial growth rates are identical to the temporal values – see the previous discussion in §3.1.

We now deduce the asymptotic structure of the strong-interaction inviscid mode as the wavenumber tends to zero. Rather than going into the detail of §3, we simply give the structure corresponding to the small-wavenumber limit of the present scaling (cf. §3.1). This is sufficient to illustrate an important dependence on γ.

5.1. *The small-$\mathscr{K}$ behaviour*

Numerical solutions of the pressure-amplitude equation, (4.36), indicate that for $\gamma = 1.4$, $\mathscr{C}$ increases as $\mathscr{K}$ tends to zero; similar behaviour was found for the far-downstream problem studied in §3. In this subsection we deduce the leading-order behaviour of $\mathscr{C}$, as $\mathscr{K} \to 0$, using scaling arguments. Such scaling arguments were employed by the authors when deducing the expansion (3.9). In fact, the small-$\hat{k}$

problem considered in §3.1 is very similar to the present problem; the former can be thought of as a special, simpler case of the latter, corresponding to the mathematical limit $\gamma \to \infty$, after the appropriate rescalings.

We begin by noting that although the WKBJ asymptote (4.37*b*) is valid if s is sufficiently large, for small $\mathscr{K}$ this form breaks down in a 'turning-point' region when

$$s \sim \mathscr{K}^{-\frac{3\gamma}{3\gamma-2}} \gg 1. \tag{5.2}$$

In this region we define

$$\hat{y} = \mathscr{K}^{\frac{3\gamma}{3\gamma-2}} s, \quad \hat{p} = \hat{P}_0(\hat{y}) + \ldots. \tag{5.3a,b}$$

Using the large-s asymptotes for G, (4.28), it follows that $\hat{P}_0$ satisfies

$$\hat{P}_{0\hat{y}\hat{y}} - A_0^2 \hat{y}^{-\frac{4}{3\gamma}} \hat{P}_0 = 0. \tag{5.4}$$

This equation has an analytic solution involving the modified Bessel function K_ν:

$$\hat{P}_0 = (4A_0\nu)^\nu \bar{D}_0 \hat{y}^{\frac{1}{2}} K_\nu(2A_0\nu\hat{y}^{\frac{1}{2\nu}}), \tag{5.5a}$$

where

$$\nu = \frac{3\gamma}{2(3\gamma-2)}, \tag{5.5b}$$

and $\bar{D}_0$ is an arbitrary constant. From the series expansion of the modified Bessel function, e.g. Abramowitz & Stegun (1964), we have that as $\hat{y} \to 0$

$$\hat{P}_0 = \frac{2^{2\nu-1}\pi\bar{D}_0}{\Gamma(1-\nu)\sin(\nu\pi)}\left(1 - \frac{\Gamma(1-\nu)(A_0\nu)^{2\nu}}{\Gamma(1+\nu)}\hat{y} + \frac{A_0^2\nu^2}{1-\nu}\hat{y}^{\frac{1}{\nu}} + \ldots\right), \tag{5.6}$$

where Γ is the Gamma function. The ordering of the second and third terms is dependent on the value of γ. For $\gamma = \frac{4}{3}$, i.e. $\nu = 1$, the powers of $\hat{y}$ of these terms are equal, while their coefficients are singular; this indicates the presence of a logarithmic term which requires special treatment.

As $\hat{y} \to 0$ the expansion (5.3) continues to be valid until contributions from the term proportional to $\hat{p}_s$ in (4.36) become significant. The scaling in this region can be deduced by analogy with the corresponding analysis of §3.1. In particular we expect $\mathscr{C} \gg 1$ as $\mathscr{K} \to 0$, and that $s \sim \mathscr{C}^{-\frac{1}{4}}$ in the new asymptotic region (see (4.27) and (4.36)). The appropriate scalings are

$$\bar{y} = \hat{\delta}^{-\frac{1}{4}} s, \quad \hat{p} = \frac{2^{2\nu-1}\pi\bar{D}_0}{\Gamma(1-\nu)\sin(\nu\pi)}(1 + \mathscr{K}^2\hat{\delta}^{-\frac{3}{2}}\bar{p}_1(\bar{y}) + \ldots), \quad \mathscr{C} = \hat{\delta}^{-1}\hat{\mathscr{C}} + \ldots, \tag{5.7a–c}$$

where $\hat{\delta} \ll 1$, $\mathscr{K}^2\hat{\delta}^{-\frac{3}{2}} \ll 1$, and the form of the expansion for $\hat{p}$ follows from the condition that (4.36) simplifies to an equation equivalent to (3.12*b*). Substitution of (5.7) into (4.36) and use of (4.27) yields

$$\bar{p}_{1\bar{y}\bar{y}} + \frac{8G_0}{\bar{y}(G_0 + \hat{\mathscr{C}}\bar{y}^4)}\bar{p}_{1\bar{y}} = \frac{G_0^2}{\bar{y}^8}. \tag{5.8}$$

As before this can be integrated to give

$$\bar{p}_{1\bar{y}} = \left(\hat{\mathscr{C}} + \frac{G_0}{\bar{y}^4}\right)^2 \left(\int_\infty^{\bar{y}} \frac{G_0^2\,\mathrm{d}\bar{y}}{(\hat{\mathscr{C}}\bar{y}^4 + G_0)^2} + \bar{D}_1\right), \tag{5.9}$$

where the constant $\bar{D}_1$ is fixed by matching to the $\hat{y} = O(1)$ region. A straightforward match is possible only if $\gamma > \frac{4}{3}$, and consistent choices of $\hat{\delta}$ and $\bar{D}_1$ are then

$$\hat{\delta}^{\frac{7}{4}} = \frac{\Gamma(1+\nu)}{\Gamma(1-\nu)\nu^{2\nu}}\mathscr{K}^{\frac{3\gamma-4}{3\gamma-2}}, \quad \bar{D}_1 = -\frac{A_0^{2\nu}}{\hat{\mathscr{C}}^2}. \tag{5.10a,b}$$

The eigenrelation for $\hat{\mathscr{C}}$ is fixed by considering a further region where $s = O(\mathscr{K}^{\frac{1}{3}})$. The details are identical to those of region IV in §3.1, and lead to the condition that $\bar{p}_{1\bar{y}} \to 0$ as $\bar{y} \to 0$. From (5.9), (5.10*b*), the eigenrelation for $\hat{\mathscr{C}}$ is thus

$$\int_0^\infty \frac{G_0^2 \,\mathrm{d}\bar{y}}{(\hat{\mathscr{C}}\bar{y}^4 + G_0)^2} + \frac{A_0^{2\nu}}{\hat{\mathscr{C}}^2} = 0 \quad \Leftrightarrow \quad \hat{\mathscr{C}} = \left(\frac{8\sqrt{2}\,A_0^{2\nu}}{3\pi G_0^{\frac{1}{2}}}\right)^{\frac{4}{7}} \exp\left(\frac{4\mathrm{i}\pi}{7}\right), \qquad (5.11a, b)$$

where as in (3.13) the unique root with $\mathrm{Im}\,(\hat{\mathscr{C}}_1) > 0$ has been chosen. This corresponds to an unstable mode of (4.36) such that the complex frequency, $\mathscr{C}\mathscr{K}$, tends to zero as $\mathscr{K}$ decreases.

The above derivation only holds if $\gamma > \frac{4}{3}$. If $\gamma = \frac{4}{3}$, then $\nu = 1$, and the small-$\hat{y}$ series (5.6) is replaced by a formula including logarithms. However, an analysis leading to (5.11) can still be carried out if (5.10*a*) is replaced by

$$\hat{\delta} = -\frac{1}{\log \mathscr{K}^2} + O\left(\frac{\log(-\log \mathscr{K}^2)}{(\log \mathscr{K}^2)^2}\right). \qquad (5.12)$$

Strictly, modifications in the same spirit are necessary if $(\gamma - \frac{4}{3}) = O(-\log \mathscr{K}^2)^{-1}$.

If $\gamma < \frac{4}{3}$ then the solution (5.5) for $\hat{y} = O(1)$ is still correct; however, it is no longer appropriate to assume that $\mathscr{C}$ is large. Therefore, for $s = O(1)$ we try the expansions

$$\mathscr{C} = \mathscr{C}_1 + \ldots, \quad \hat{p} = 1 + \ldots + \mathscr{K}^2 \hat{p}_1 + \ldots, \qquad (5.13a, b)$$

which lead to the governing equation

$$\hat{p}_{1ss} - \frac{2G_s}{G - \mathscr{C}_1}\hat{p}_{1s} = G^2. \qquad (5.13c)$$

If the solution to this equation is to match both with that for $\hat{y} = O(1)$, and the solution in the $s = O(\mathscr{K}^{\frac{1}{3}})$ layer (region IV), then the eigenrelation

$$\int_0^\infty \frac{G^2}{(G - \mathscr{C}_1)^2}\,\mathrm{d}s = 0 \qquad (5.14)$$

must be satisfied. A numerical solution of (5.14) for a typical value of $\gamma = 1.1$ ($< \frac{4}{3}$) determined $\mathscr{C}_1 = (-0.06226, 0.1343)$, which was found to be in close agreement with the small-$\mathscr{K}$ behaviour of the solution to (4.36) and (4.37) for the same value of γ.

Although the above asymptotic solutions for small $\mathscr{K}$ have been derived for the small-x pressure equation (4.36), similar expansion can be obtained for the $x = O(1)$ Rayleigh equation (4.34).

5.2. *Large-wavelength vorticity modes*

A natural question to ask is: how is the above asymptotic solution modified when the wavelength becomes sufficiently long that a new physical effect needs to be included? One possibility is that once the modes become comparable in length with the thickness of the boundary layer, and hence with the inviscid layer, a rescaling in the spirit of §3.2 is necessary – but additionally including the direct effect of the shock (see Brown *et al.* 1991 for a particular limiting case). Another possibility is that neglected non-parallel effects come into play (cf. Smith 1989; Blackaby 1991; Brown *et al.* 1991). However, it turns out that at least for $\gamma > \frac{4}{3}$ neither of these physical effects is the first that needs to be included as the wavelength increases. Instead, scaling arguments indicate that once $\alpha \sim M^{-\frac{7(3\gamma-2)(8-3\gamma)}{3(6\gamma-1)(6-\gamma)}}$, the x-derivative of normal blowing velocity, (4.14), can no longer be neglected as far as the calculation of the leading-order *eigenvalue* is concerned (in our earlier calculations the blowing velocity

could be shown to be asymptotically negligible as far as the instability analysis was concerned). Moreover, it turns out that the *eigenfunction* is significantly altered before α becomes this small.

A full examination of this new effect will be given elsewhere. Here we outline aspects of the analysis, indicating how for $\gamma > \frac{4}{3}$ the blowing velocity changes the growth rate at leading order. In this subsection we choose to consider the temporal stability case for the sake of simplicity. Unfortunately, while it is easy to identify the new physical effect that needs to be included, the analysis leading to the correct growth rate is algebraically messy – partly because the full flow is described by six asymptotic regions. However, as far as the instability analysis is concerned, the four main regions are just scaled versions of those illustrated in figure 4.

Scaling arguments suggest that in all the regions it is appropriate to redefine the 'fast' variables as (cf. (4.30)):

$$X = M^{\frac{3\gamma+14}{3(6-\gamma)}}(x-t), \quad Z = M^{\frac{3\gamma+14}{3(6-\gamma)}}z, \quad \tau = M^{\frac{3\gamma-2}{3(6-\gamma)}}t. \tag{5.15a–c}$$

In layer I, we introduce a scaled coordinate

$$\hat{y} = M^{\frac{6+\gamma}{6-\gamma}}\psi, \tag{5.16a}$$

while the velocity, density, temperature and pressure expand as follows:

$$(u,v,w,p) = (1-M^{-\frac{2(16-3\gamma)}{3(6-\gamma)}}\bar{A}_0\hat{y}^{-\frac{2}{3\gamma}}, M^{-1}V_{1\infty}, 0, M^{-2}P_1)+\ldots + M^{\frac{20}{3(6-\gamma)}}(\hat{U}_0,\hat{V}_0,\hat{W}_0,M^{-\frac{20}{3(6-\gamma)}}\hat{P}_0)+\ldots, \tag{5.16b}$$

$$(\rho,T) = (M^{-\frac{4}{3(6-\gamma)}}\gamma(\gamma-1)^{-1}\bar{A}_0^{-1}P_1\hat{y}^{\frac{2}{3\gamma}}, M^{\frac{4}{3(6-\gamma)}}(\gamma-1)\bar{A}_0\hat{y}^{-\frac{2}{3\gamma}})+\ldots+(M^{\frac{32}{3(6-\gamma)}}\hat{R}_0, M^{\frac{40}{3(6-\gamma)}}\hat{T}_0)+\ldots, \tag{5.16c}$$

where the first terms are the steady flow contributions, the circumflexed variables describe the linear unsteady perturbation,

$$V_{1\infty} = v_1(x,0), \quad \text{and} \quad \bar{A}_0(x) = \frac{\gamma}{\gamma-1}[p_1(x,0)]^{\frac{\gamma-1}{\gamma}}(e_1^3 a_1^8)^{\frac{1}{3\gamma}}. \tag{5.16d,e}$$

We also assume that the rapid variation of the unsteady perturbation has a WKBJ form; hence to leading order

$$\hat{U}_{0X} = \mathrm{i}\alpha\hat{U}_0, \quad \hat{U}_{0Z} = \mathrm{i}\beta\hat{U}_0, \quad \hat{U}_{0\tau} = -\mathrm{i}\alpha\hat{c}\hat{U}_0, \quad \text{etc.}, \tag{5.17}$$

where α, β and $\hat{c}$ are functions of the slow variable x. On substitution into the governing equations (2.2), the leading-order equation for the linear pressure perturbation is found to be

$$\left(\frac{\hat{P}_{0\hat{y}}}{1+\frac{2}{3}P_1V'_{1\infty}(\gamma-1)^{-1}\bar{A}_0^{-1}\alpha^{-2}\hat{c}^{-2}\hat{y}^{-(3\gamma-2)/3\gamma}}\right)_{\hat{y}} - \frac{(\alpha^2+\beta^2)(\gamma-1)^2\bar{A}_0^2}{\gamma^2P_1^2\hat{y}^{4/3\gamma}}\hat{P}_0 = 0, \tag{5.18}$$

where $V'_{1\infty}$ is the x-derivative of $V_{1\infty}$ – from (4.5c) and (4.14) this is negative for small x, and is expected to be so for all x. Equation (5.18) is analogous to (5.4), which is recovered on setting $V'_{1\infty} = 0$ except for scaling factors. We discuss the solution of this equation after deriving the governing equations in the other layers.

In layer IV, the appropriate normal coordinate is

$$\hat{\xi} = M^{\frac{166-33\gamma}{9(6-\gamma)}}\psi, \tag{5.19a}$$

while the velocity, density, temperature and pressure expand as:

$$(u,v,w,p) = (1-M^{-\frac{8(3\gamma-2)}{9(6-\gamma)}}g_0\hat{\xi}^{-4}, M^{-1}V_{1\infty}, 0, M^{-2}P_1)+\ldots+M^2(\hat{u},\hat{v},\hat{w},M^{-2}\hat{p})+\ldots,$$

(5.19*b*)

$$(\rho, T) = (M^{-\frac{2(62-21\gamma)}{9(6-\gamma)}}\gamma(\gamma-1)^{-1}g_0^{-1}P_1\,\hat{\xi}^4, M^{\frac{2(62-21\gamma)}{9(6-\gamma)}}(\gamma-1)\,g_0\,\hat{\xi}^{-4}) + \ldots + (M^{\frac{16(3\gamma-2)}{9(6-\gamma)}}\hat{\rho}, M^4\hat{T}) + \ldots . \tag{5.19c}$$

The governing equation for the pressure perturbation $\hat{p}$ is found to be

$$\hat{p}_{\hat{\xi}\hat{\xi}} + \frac{8\hat{p}_{\hat{\xi}}}{\hat{\xi}} - \frac{(\alpha^2+\beta^2)(\gamma-1)^2 g_0^2}{\gamma^2 P_1^2\,\hat{\xi}^8}\hat{p} = 0. \tag{5.20}$$

Except for a rescaling, this is (3.12*d*).

The scalings in layer III are

$$\tilde{\xi} = M^{\frac{50-9\gamma}{3(6-\gamma)}}\psi, \tag{5.21a}$$

$$(u, v, w) = (1 - M^{-\frac{16}{3(6-\gamma)}}g_0\,\tilde{\xi}^{-4}, M^{-1}V_{1\infty} + M^{-\frac{3(10-\gamma)}{3(6-\gamma)}}v_1, 0) + \ldots$$
$$+ (M^2(\tilde{u}_0 + \ldots + \epsilon\tilde{u}_1), M^{\frac{20}{3(6-\gamma)}}(\tilde{v}_0 + \ldots + \epsilon\tilde{v}_1), M^2(\tilde{w}_0 + \ldots + \epsilon\tilde{w}_1)) + \ldots, \tag{5.21b}$$

$$p = M^{-2}P_1 + \ldots + \tilde{p}_0 + \ldots + \epsilon\tilde{p}_1 + \ldots + \epsilon^2\tilde{p}_2 + \ldots, \tag{5.21c}$$

$$(\rho, T) = (M^{-\frac{20-6\gamma}{3(6-\gamma)}}\gamma(\gamma-1)^{-1}g_0^{-1}P_1\,\tilde{\xi}^4, M^{\frac{20-6\gamma}{3(6-\gamma)}}(\gamma-1)\,g_0\,\tilde{\xi}^{-4}) + \ldots$$
$$+ (M^{\frac{32}{3(6-\gamma)}}(\tilde{\rho}_0 + \ldots + \epsilon\tilde{\rho}_1), M^4(\tilde{T}_0 + \ldots + \epsilon\tilde{T}_1)) + \ldots, \tag{5.21d}$$

where

$$\tilde{p}_{0\tilde{\xi}} = 0, \quad \epsilon = M^{-\frac{2(8-3\gamma)}{3(6-\gamma)}}. \tag{5.21e}$$

Strictly, further terms should be included both (*a*) in the steady part of the perturbation series arising from the expansion for asymptotic small values of $\eta = O(M^{-\frac{(8-3\gamma)(3\gamma-4)}{3(6\gamma-1)(6-\gamma)}})$ of the adjustment layer function, $\bar{G}$ (see (2.10*c*)), and (*b*) in the unsteady part of the series due to a variety of forcing terms. In addition, the scaled phase speed, $\hat{c}$, and wavenumbers, α, β, should also be expanded in powers of ϵ, etc. However, we believe that the terms retained are those which yield the correct leading-order secularity condition.

On substituting into (2.2), we find after some manipulation and matching with layer IV that

$$\tilde{p}_{1\tilde{\xi}} = \frac{4(\gamma-1)\,g_0\,V'_{1\infty}}{\gamma P_1}\left(\frac{\alpha^2+\beta^2}{\alpha^2}\right)\tilde{p}_0\,\tilde{\xi}^3\int_0^{\tilde{\xi}}\frac{\mathrm{d}\tilde{\xi}}{(g_0+\hat{c}\tilde{\xi}^4)^2}, \tag{5.22a}$$

while

$$\tilde{p}_{2\tilde{\xi}} = \frac{4(\gamma-1)\,g_0\,V'_{1\infty}}{\gamma P_1}\left(\frac{\alpha^2+\beta^2}{\alpha^2}\right)\tilde{\xi}^3\int^{\tilde{\xi}}\frac{\tilde{p}_1\,\mathrm{d}\tilde{\xi}}{(g_0+\hat{c}\tilde{\xi}^4)^2}$$
$$+ \frac{(\gamma-1)^2 g_0^2}{\gamma^2 P_1^2}\left(\frac{g_0+\hat{c}\tilde{\xi}^4}{\tilde{\xi}^4}\right)^2(\alpha^2+\beta^2)\,\tilde{p}_0\int^{\tilde{\xi}}\frac{\mathrm{d}\tilde{\xi}}{(g_0+\hat{c}\tilde{\xi}^4)^2}, \tag{5.22b}$$

where the precise lower limits in the integrals are not needed in order to determine the leading-order eigenvalue.

In region II the expansions are very similar to those above. On writing

$$p = M^{-2}P_1 + \ldots + \check{p}_0 + \ldots + \epsilon\check{p}_1 + \ldots, \tag{5.23a}$$

we find after some algebraic manipulation, and matching with layer III using (5.22*a*), that

$$\check{p}_{1\eta} = -\frac{V'_{1\infty}\,\bar{T}_\eta}{\bar{T}^2}\left(\frac{\alpha^2+\beta^2}{\alpha^2}\right)\tilde{p}_0\frac{(\gamma-1)^2 g_0^2}{\gamma P_1}\int_0^\infty\frac{\mathrm{d}\tilde{\xi}}{(g_0+\hat{c}\tilde{\xi}^4)^2}, \tag{5.23b}$$

where $\bar{T}$ is the steady temperature field as given by (3.1*b*).

The eigenvalue problem is now fixed by matching with layer I. We find that the pressure perturbation in this layer must satisfy the governing equation (5.18), together with the boundary conditions

$$\hat{P}_0 \to 0 \quad \text{as} \quad \hat{y} \to \infty, \tag{5.24a}$$

$$\hat{P}_0 \to \tilde{p}_0\left(1+\hat{B}\left\{\hat{y}^{\frac{2}{3\gamma}}+\frac{(\gamma-1)\bar{A}_0\alpha^2\hat{c}^2}{\gamma P_1 V'_{1\infty}}\hat{y}\right\}\right) \quad \text{as} \quad \hat{y}\to 0, \tag{5.24b}$$

where

$$\hat{B} = \frac{(\gamma-1)g_0^2}{\gamma\bar{A}_0 P_1}V'_{1\infty}\left(\frac{\alpha^2+\beta^2}{\alpha^2}\right)\int_0^\infty \frac{\mathrm{d}\tilde{\xi}}{(g_0+\hat{c}\tilde{\xi}^4)^2}. \tag{5.24c}$$

In general this appears to require a numerical solution. However, it is easy to verify that as $\alpha\to\infty$ the eigenvalue (5.11) is recovered. It is also possible to recover an asymptotic solution as $\alpha\to 0$. To this end we introduce the scaled coordinate

$$\hat{Y} = \Lambda^{-1}\hat{y}, \tag{5.25a}$$

where

$$\Lambda = \left(\frac{3\gamma^2\alpha^2\hat{c}^2 P_1}{2(\gamma-1)(\alpha^2+\beta^2)\bar{A}_0 V'_{1\infty}}\right)^{\frac{3\gamma}{3\gamma-2}}, \tag{5.25b}$$

and for definiteness

$$\arg(V'_{1\infty}) = \pi, \quad 0 < \arg(\hat{c}) < \pi. \tag{5.25c}$$

The governing equation then becomes

$$\left(\frac{\hat{P}_{0\hat{Y}}}{\hat{Y}^{-(3\gamma-2)/3\gamma}+\frac{9}{4}\alpha^4(\alpha^2+\beta^2)^{-1}\hat{c}^4\gamma^2(V'_{1\infty})^{-2}}\right)_{\hat{Y}} - \frac{\hat{P}_0}{\hat{Y}^{\frac{4}{3\gamma}}} = 0, \tag{5.25d}$$

with boundary conditions (5.24*a*) and

$$\hat{P}_0 \to \tilde{p}_0\left(1+\check{B}\left\{\hat{Y}^{\frac{2}{3\gamma}}+\frac{3\gamma\alpha^4\hat{c}^4}{2(\alpha^2+\beta^2)V'^2_{1\infty}}\hat{Y}\right\}\right) \quad \text{as} \quad \hat{Y}\to 0, \tag{5.25e}$$

where

$$\check{B} = (\tfrac{3}{2}\hat{c}^2)^{\frac{2}{3\gamma-2}}\left(\frac{(\alpha^2+\beta^2)(\gamma-1)\bar{A}_0 V'_{1\infty}}{\alpha^2\gamma^2 P_1}\right)^{\frac{3\gamma-4}{3\gamma-2}}\frac{3\pi\gamma g_0^{\frac{1}{4}}}{8\sqrt{2}\,\bar{A}_0^2\hat{c}^{\frac{1}{4}}}. \tag{5.25f}$$

As α, $\beta\to 0$, it can be confirmed from (5.27) that $\alpha^4\hat{c}^4/(\alpha^2+\beta^2)\to 0$, and hence the appropriate solution to (5.25*d*) that decays exponentially at infinity for the choice of arguments specified by (5.25*c*) is

$$\hat{P}_0 \propto \hat{Y}^{\frac{1}{3\gamma}}K_\nu\left(\frac{6\gamma}{3\gamma-2}\hat{Y}^{\frac{3\gamma-2}{6\gamma}}\right), \tag{5.26}$$

where we have now set $\nu = 2/(3\gamma-2)$. From matching with (5.25*e*,*f*) it follows from the small-$\hat{Y}$ expansion of K_ν that

$$(\tfrac{3}{2})^{\frac{2}{3\gamma-2}}\left(\frac{(\alpha^2+\beta^2)(\gamma-1)\bar{A}_0 V'_{1\infty}}{\alpha^2\gamma^2 P_1}\right)^{\frac{3\gamma-4}{3\gamma-2}}\left(\frac{3\gamma-2}{3\gamma}\right)^{2\nu}\frac{3\pi\gamma g_0^{\frac{1}{4}}\Gamma(1+\nu)}{8\sqrt{2}\,\bar{A}_0^2\Gamma(1-\nu)}\hat{c}^{\frac{3(6-\gamma)}{4(3\gamma-2)}} = -1. \tag{5.27}$$

If $\frac{4}{3} < \gamma < \frac{10}{3}$ (in fact if $1 < \gamma < \frac{10}{3}$), this has a unique solution for $\hat{c}$ satisfying (5.25*c*).

Again, as in §5.1, it is possible to examine the small-x limit of this eigenrelation, and to recover numerical values. However, we believe that the major contribution of this part of the analysis is to emphasize that the (gradient of the) blowing velocity can have a direct impact on the instability waves for modes with an $O(M^{\frac{(3\gamma-2)}{3(6-\gamma)}})$ growth

rate. From (4.30c) and (5.15c) we see that such modes have a smaller growth rate than the fastest growing modes by a factor of $M^{-\frac{(9\gamma+2)(8-3\gamma)}{3(6-\gamma)(6\gamma-1)}}$, i.e. $M^{-0.54\ldots}$ for $\gamma = 1.4$. We emphasize that because the effect of the blowing velocity is not allowed for in the compressible Orr–Sommerfeld or Rayleigh equations, its necessary inclusion here indicates that analyses based on these classical equations, e.g. quasi-parallel stability analyses of solutions of the parabolized compressible, Navier–Stokes equations, may produce erroneous results.

Finally, we note that these modes have wavelengths much larger than the thickness of the adjustment region, but much less than the width of the inviscid layer or the boundary layer. The behaviour of these modes when they have wavelengths comparable with the thickness of the boundary layer, so that they can interact with the shock, is a matter of current study. However, since these modes have growth rates significantly less than that of the fastest growing mode they might not be excited in a practical situation.

6. Summary and numerical comparisons

The primary aim of the present paper has been to investigate aspects of the inviscid instability of hypersonic boundary layers without making some of the assumptions which might lead to important aspects of the instability structure being overlooked. In particular we have attempted to determine the effects of both a realistic viscosity law and the presence of shocks on a particular class of instability wave, although we have neglected real-gas effects and have made the simplifying assumption that the Prandtl number is equal to one. The Sutherland viscosity law used is thought to be more appropriate than Chapman's linear viscosity law at the high temperatures relevant to a hypersonic boundary layer, whilst shocks are usually present in hypersonic flows of practical importance. The inviscid modes discussed are, for the most part, associated with the generalized inflexion point of the basic flow. For instance, the upper-branch neutral mode of the most rapidly growing disturbance has a wave speed equal to the flow speed at the generalized inflexion point.

In §3 we solved the inviscid instability problem for a hypersonic boundary layer far downstream of any shock; Grubin & Trigub (1993a, b) have independently carried out a closely related study. As in SB we found that the most unstable disturbance is a so-called 'vorticity mode' with wavelength comparable with the thickness of the temperature adjustment layer. This mode is destabilized by wall cooling, and an oblique mode has a smaller growth rate than a two-dimensional one. As the wavenumber is reduced, the growth rate decreases and the disturbance velocity fields spreads out from the adjustment layer. When the wavelength is comparable with the thickness of the viscous boundary layer, the eigenfunction of the instability mode is distributed throughout the boundary layer.† At a sequence of eigenvalues (at which neutral acoustic modes can be found), the growth rate decreases significantly; it is this phenomenon that is responsible for the local maxima in growth rate identified by Mack (1969). In the neighbourhood of the eigenvalues, the precise form of the dispersion relation depends on the size of a constant, d_0, associated with the solvability condition for (A 7c).

† Mack (1969, 1984, 1987) refers to such modes as acoustic modes. In order to distinguish between the two different types of acoustic modes, i.e. those described in §3.2 and the very small growth-rate modes discussed in the Appendix, we refer to the acoustic modes of §3.2 by the asymptotically equivalent title of long-wavelength vorticity modes.

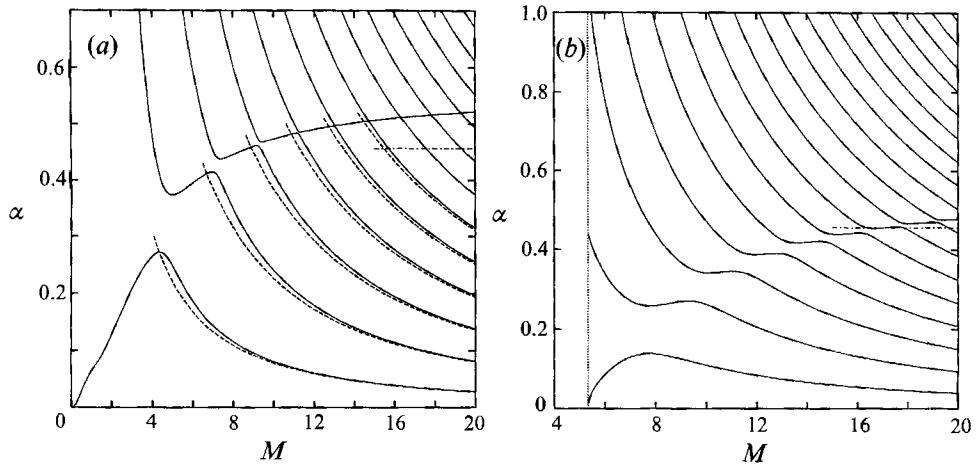

FIGURE 11. Neutral curves for modes propagating at the same velocity as fluid at the generalized inflexion point (——), and the asymptotic limit of the neutral, upper-branch vorticity mode (– · –). (*a*) Insulated wall. Asymptotic prediction of the neutral acoustic modes from (3.15*b*) (– – –). (*b*) Wall cooled to the free-stream temperature.

One possibility is that close to these eigenvalues another mode exists (e.g. see figure 15(*a*) in the Appendix, and the curve between α_{11} and α_{s1} in figure 9(*a*) of Mack 1987). While this mode has a growth rate comparable to the long-wavelength vorticity mode in the neighbourhood of the eigenvalues, the long-wavelength vorticity mode has a significantly larger growth rate away from the eigenvalues. Another possibility is that there is no second distinct mode in the neighbourhood of the eigenvalues, but that the long-wavelength vorticity mode terminates and restarts as a neutral mode (see figures 15*b* and 15*c*, and the curves emanating from α_{12} and α_{s2} in figure 9(*a*) of Mack 1987).

As the wavenumber decreases further the growth rate of the two-dimensional vorticity mode increases again (but see Grubin & Trigub 1993*b* for the case of sufficiently small Prandtl numbers). For even smaller wavenumbers, a lower-branch neutral mode can be found which has the form of a non-decaying sound wave far from the wall. For sufficiently oblique waves, a match with the smaller-growth-rate Tollmien–Schlichting waves can be achieved. For these modes viscosity cannot be neglected and the disturbance flow field takes on the structure given by Smith (1989) and Gajjar & Cole (1989).

In order to compare our high-Mach-number, asymptotic predictions with finite-Mach-number calculations we have solved Rayleigh's equation (2.12*a*) using two independent numerical schemes for basic flow solutions to (2.5) and (2.7) with $\gamma = 1.4$ and $\check{C} = 0.509$. In figure 11 we have plotted the neutral curves for modes propagating at the same velocity as fluid at the generalized inflexion point for both an insulated wall and a wall cooled to the temperature of the free stream. In figure 11(*a*) the dashed lines represent the eigenvalues for neutral acoustic modes as given by (3.15*b*); as in CH there is excellent agreement between the asymptotic theory and the numerical solution for the neutral acoustic modes. The (discontinuous) rising line in both figures is the upper-branch neutral curve for the vorticity mode. From beneath (3.7*b*), and accounting for a factor of $\sqrt{2}$, we see that it should tend to 0.456 130 for large M (marked as a dash-dot line on the right-hand side of the figure). Clearly the agreement is not outstanding (especially in the case of figure 11*a*), with

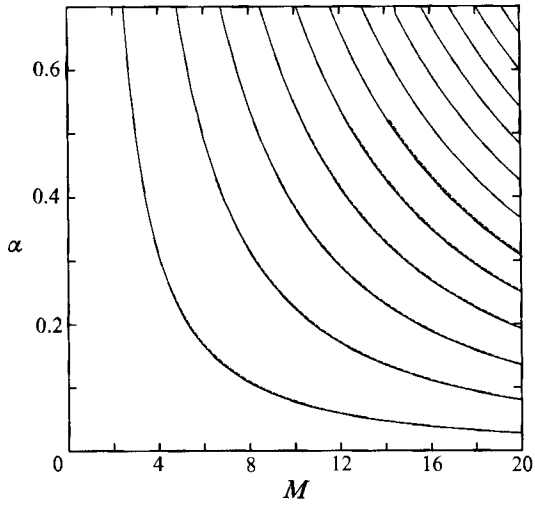

FIGURE 12. Neutral curves for modes propagating at the same velocity as the freestream. Insulated wall. Asymptotic prediction of the neutral acoustic modes from (3.15*b*) (– – –).

the trend being in the wrong direction at $M = 20$, i.e. past the upper limit at which real-gas effects, etc., should probably introduced into the analysis. The difference between the asymptotic and numerical results is in fact comparable with that obtained for Chapman's law if only the leading term in the asymptotic expansion is used. SB obtained improved agreement by taking further terms in the asymptotic series. Such an approach is not pursued here, although we note that the discrepancy may arise because the asymptotic steady solution does not predict the position of the generalized inflexion point very accurately. For instance, in the case of the insulated wall, the inflexion point for $M = 20$ is at $\eta = 2.536$ compared with the large-M asymptotic value of $\eta = 2.270$. Moreover, that $M = 20$ is too low to pick up the full asymptotic structure (at least for the insulated wall) is indicated by the fact that the lower neutral branch (i.e. $\alpha \sim 111 M^{-\frac{5}{2}}$ from §3.4) and the asymptotic eigenvalue of the lowest neutral acoustic mode (i.e. $\alpha \sim 2.47 M^{-\frac{3}{2}}$ from §3.2) are only correctly ordered for $M > 44.9$.

Figure 12 is a plot of the neutral curves for modes propagating at the same velocity as the free stream for an insulated wall. The dashed lines represent the eigenvalues (3.15*b*); again there is excellent agreement between the asymptotic theory and the numerical solution.

In figure 13 the growth rate is plotted against wavenumber for the most rapidly growing temporal mode. Figures 13(*a*) and 13(*b*) are for an insulated wall, and a wall cooled to the free-stream temperature, respectively; in both cases $M = 20$. Figure 13(*c*) is for an insulated wall at $M = 14$. The growth rates of seven other modes have also been plotted in figure 13(*a*); these modes are close to the neutral-acoustic mode wavelengths given in figures 11(*a*) and 12, but the growth rates are so small that the curves do not show up on the figure. The dashed curves in figure 13(*a–c*) are scaled versions of figure 2.

From figure 13(*a*) it appears that for an insulated wall the most rapidly growing mode at $M = 20$ is essentially the vorticity mode; we conclude that the analysis of §3.1 captures many of the important features of the instability. However, the wall temperatures are unrealistically high in this case for the result to be physically useful. Further, the Mach number does not seem to be sufficiently large for there to

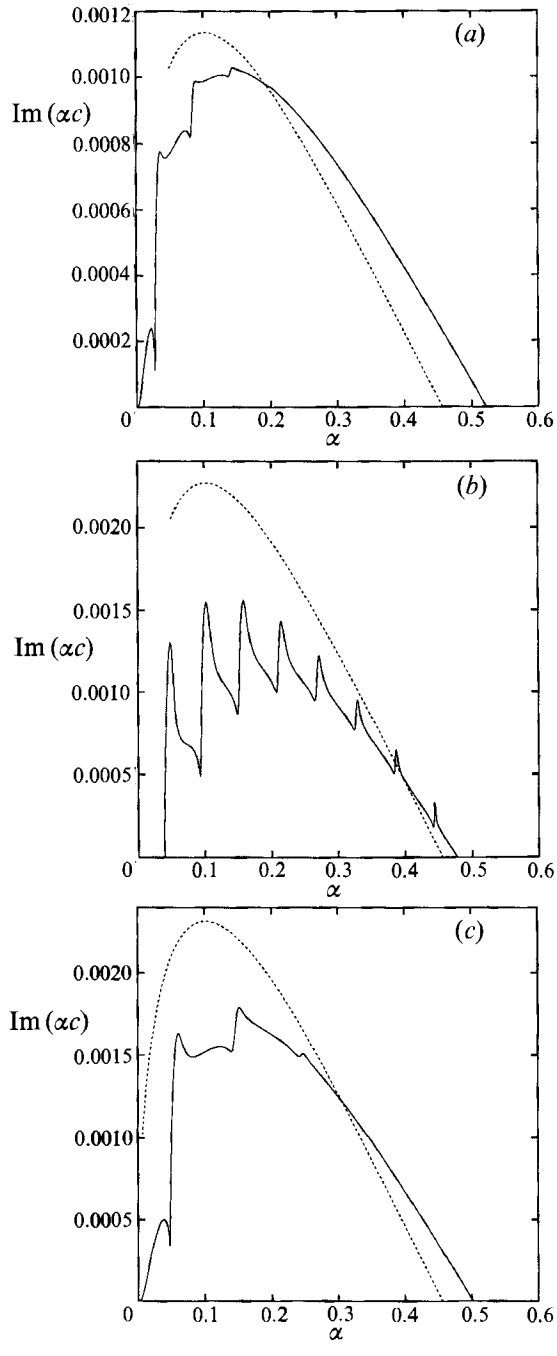

FIGURE 13. Growth-rate curves both for numerical solutions to Rayleigh's equation (— —), and from a scaled version of figure 2 (- - -). (*a*) $M = 20$ and an insulated wall. Eight numerical solutions are plotted, seven of which are graphically indistinguishable from the abscissa. (*b*) $M = 20$ and a wall cooled to the free-stream temperature. (*c*) $M = 14$ and an insulated wall.

be the clear separation of scales illustrated schematically in figure 7. As a result, the overlapping acoustic modes reduce the maximum growth rate, and there is no clear non-acoustic mode minimum (§3.3). There is also no lower branch neutral mode at a finite wavenumber (§3.4); instead

$$c \to 1 - 1/M \quad \text{as} \quad \alpha \to 0. \tag{6.1}$$

A small-wavenumber asymptotic analysis of such neutral sonic modes was given by SB. As there, we anticipate that such a structure can only hold for finite Mach numbers, and that at sufficiently large values of M the structure of §3.4 is recovered.

The quantitative agreement between the asymptotic analysis and the numerical results is less good in figures 13(*b*) and 13(*c*). However, the qualitative agreement suggests that the asymptotic analysis has captured key features of the physics.

7. Discussion

The result that the temperature adjustment layer is the site of the most rapidly growing inviscid disturbance is consistent with the observation that transition is initiated in the outer part of a hypersonic boundary layer (e.g. Fischer & Weinstein 1972). Moreover, a vortex-wave-interaction calculation with the vorticity wave as one of the components (cf. Hall & Smith 1991; Blackaby 1991) may describe the rope-like structures observed at the boundary-layer edge.

Regarding numerical calculations, the fact that the most unstable mode is concentrated in the physically thin adjustment layer suggests that it will only be possible to describe the structure of this mode if the basic steady flow is known to high accuracy. In addition the concentration of the disturbance in the adjustment layer is in line with the work of Fu *et al.* (1990) for Görtler vortex instability of Sutherland-law, hypersonic-boundary-layer flow over curved walls. In that problem it was shown that a hypersonic boundary layer could support modes associated with the wall layer and the temperature adjustment layer. The fastest growing mode was shown to be concentrated in the adjustment layer and described at zeroth order by quasi-parallel theory; in fact the most unstable type of Görtler vortex is inviscid and has a growth rate larger than that of the vorticity mode. The wall-layer mode for Görtler vortices is controlled by non-parallel effects unlike its counterpart, the 'acoustic' mode, discussed here.

The other likely cause of transition in a compressible boundary layer, i.e. Tollmien–Schlichting waves, can only occur when they are three-dimensional and propagate outside the Mach-wave cone (Smith 1989). Furthermore these waves are largely uninfluenced by the temperature adjustment layer because Tollmien–Schlichting waves are induced by viscosity in a thin layer located at the bottom of the wall layer. Since the growth rates associated with the vorticity mode discussed here, and the Görtler mode discussed by Fu *et al.* (1990), are larger than those of the Tollmien–Schlichting waves, it seems likely that transition in hypersonic boundary layers will occur first in the temperature adjustment layer – that is assuming that the receptivity mechanism generating the instabilities in the adjustment and wall layers produces comparable amplitudes for the different modes. That might not be the case if wall roughness plays a significant role in the process.

Given that the asymptotic analysis for the vorticity mode seems to pick up the dominant instability features, we have examined the instability to such disturbances of the steady flow in the strong-interaction region near the leading edge. Our results are the first to show the influence of the attached leading-edge shock on such an

inviscid mode in the strong-interaction region. We find that while the shock is too far away from the adjustment layer to have a direct effect on the most rapidly growing mode, its influence is felt through the basic state which is fundamentally altered by the presence of the shock.

While the vorticity-mode eigenvalue problem was formulated in the region where the hypersonic interaction parameter is $O(1)$, it was not solved there. This is because, to the authors' knowledge, the basic flow in this regime has not been calculated numerically despite having been formulated some years ago (e.g. Luniev 1959). Instead we chose to consider the strong-interaction regime where a similarity solution for the basic state is available. However, once the recent numerical calculations by Brown *et al.* (1991) for the full interaction problem are modified to use the Sutherland formula, rather than Chapman's law, then it will be relatively straightforward to extend our calculations to the $O(1)$ interaction region.

Our analysis for the strong-interaction-problem vorticity mode showed that, at a fixed x-station, a fastest growing vorticity mode exists for a finite value of the wavenumber when the latter is scaled on the adjustment-layer thickness. In §5 we derived the small-wavenumber form of this mode. For sufficiently small wavenumbers we find that the correct growth rate is only recovered if the *normal velocity component* of the basic state is included in the analysis. Moreover, this occurs both before the direct influence of the shock is felt, and before the 'acoustic' modes are recovered. This suggests that near the leading edge, a stability analysis based on the compressible Orr–Sommerfeld equation could be misleading, since important terms related to the non-zero, steady velocity normal to the plate are conventionally omitted from this equation.

Recently Malmuth (1991) and Brown *et al.* (1991) have looked at the possibility that the inviscid flow adjacent to the shock can itself be unstable. Malmuth (1991) studied disturbances with streamwise lengthscales comparable with the length of the steady interaction region, while Brown *et al.* (1991) considered disturbances with streamwise lengthscales comparable with the width of the shock layer (but also accounting for a slower spatial development). In both papers the wall and adjustment layers are assumed to be passive, even though it is not immediately clear that such an assumption is justifiable since the disturbed flow persists in these regions. As a result of that assumption, the modes described in the present paper are specifically excluded from both analyses.

However, instabilities which owe their origin to the existence of the shock may be important and should be studied. This is especially so in flows where highly curved shocks are present as a result of flow around blunt bodies; there must be intentional blunting of the leading surfaces in hypersonic vehicles due to heat transfer considerations. We note that Reshotko & Khan (1979) have considered the stability of laminar supersonic flow over a blunt plate. Based on experimental results for the location of transition, they considered the stability problem far downstream from the nose of the body. They attempted to assess how the flow instability depends on the ratio of the local boundary-layer thickness to the radius of the nose. In our notation (see the end of §1), they essentially considered a 'weak' hypersonic limit; for example the scaling $R = O(M^8)$ where the non-uniform part of the inviscid layer is absorbed into the boundary layer. In contrast we have considered instabilities in the strong-interaction zone. In particular, for a flat plate we have demonstrated the existence of disturbances further upstream than those considered by Reshotko & Khan (1979) for a blunt plate. We believe that it should be relatively straightforward to modify aspects of our analysis in order to consider a blunt plate, or even a blunt cone.

However, until this is done we are unable to properly compare our theory with the results of Reshotko & Khan (1979).

Finally we make a few remarks about how the results of the present study should be interpreted with respect to any experimental investigation of transition in a hypersonic boundary layer. Firstly, we note that both the spatial and temporal instability problems have been treated. Unless the instability is forced over a significant streamwise extent we expect that the spatially growing modes would be the ones excited. Secondly, while we have not addressed the receptivity problem, for a broadband disturbance we expect the most unstable mode, i.e. the vorticity mode, to lead to transition. However, there may be circumstances in which the excitation frequency does not match the frequency of the vorticity mode. For this reason we have mapped out the asymptotic structure of the instability modes over a wide range of frequencies and wavenumbers. In particular, because the most rapidly growing vorticity mode decays exponentially away from the adjustment layer, in an experiment where disturbances are stimulated near the wall it could be that longer wavelength (lower frequency) modes which extend to the wall are preferentially excited to the extent that the most unstable modes never reach a critical amplitude before transition occurs. Presumably this is one of the reasons why Goldstein & Wundrow (1990) studied the nonlinear evolution of near-neutral acoustic modes, even though they have significantly smaller growth rates than the neighbouring vorticity mode (but see also the comment at the end of the Appendix and the recent paper by Wundrow 1992). Thirdly, we note that the instability problems for different locations downstream have been treated in isolation from each other. We are able to do this because the temporal and spatial scales for the disturbances in the different regions are different; hence it is only necessary to look at the instability problem for a wave of a given frequency in a region where it is potentially unstable. In an experiment where many possible frequencies are available through the background disturbance field, transition will probably be caused by the disturbances that are amplified closest to the leading edge.

The authors wish to thank Dr A. P. Bassom for his assistance with the numerical solution of the wall-layer equation. N.D.B. and P.H. wish to acknowledge the Science and Engineering Research Council of Great Britain for financial support. S.J.C. wishes to thank the Mathematical Sciences Institute of Cornell University and the Institute of Computational Mechanics and Propulsion for financial support. The authors would also like to thank the Institute for Computer Applications in Science and Engineering, and NASA Langley Research Centre for financial support and hospitality whilst part of this research was carried out. Versions of this paper were presented at the 31st BTMC (Exeter, April 1989), the 3rd Symposium on Laminar–Turbulent Transition (Toulouse, September 1989), and the 32nd BTMC (St Andrews, April 1990). A preprint appeared as *ICASE Rep.* 90-40.

Appendix

In order to examine the structure of the long-wavelength vorticity mode in the neighbourhood of the eigenvalues (3.15*b*), we expand the wavenumbers (α, β) in the form

$$(\alpha, \beta) = \frac{1}{M^{\frac{3}{2}}}(\alpha_0^*, \beta_0^*) + \frac{1}{M^{\frac{25}{14}}}(\alpha_1^*, \beta_1^*) + \ldots, \qquad (A\,1a)$$

where (α_0^*, β_0^*) are an eigenvalue pair of (3.14*b*); c still expands as in (3.15*a*). We begin by determining the temporal growth rate when the wavenumber perturbation (α_1^*, β_1^*) is non-zero. In the wall layer $\tilde{p}$ expands as

$$\tilde{p} = M^{\frac{2}{7}} Q_0 + \ldots + Q_1 + \ldots, \tag{A 1b}$$

where we have anticipated the possible occurrence of further terms between Q_0 and Q_1. For instance these might include scaled multiples of Q_0 forced by higher-order terms in the expansion for the mean velocity; however, for our purposes it is not necessary to calculate them here. If we substitute (A 1*b*) into Rayleigh's equation we see that Q_0 satisfies (3.14*b*) with $(\alpha, \beta) = (\alpha_0^*, \beta_0^*)$; in addition $Q_0'(0) = 0$, whilst

$$Q_0 \sim q_0 \xi^{-7} \quad \text{for} \quad \xi \gg 1; \tag{A 1c}$$

q_0 is a constant which, without any loss of generality, can be set equal to unity in order to normalize the eigenfunction Q_0. At higher order in Rayleigh's equation we find that Q_1 satisfies

$$\begin{aligned} Q_1'' - \frac{2\bar{u}_0'}{\bar{u}_0 - 1} Q_1' - \tfrac{1}{4}(\gamma-1)^2 (T_b + \bar{u}_0)^2 (1-\bar{u}_0)^2 \left((\alpha_0^{*2} + \beta_0^{*2}) - \frac{2\alpha_0^{*2}(1-\bar{u}_0)}{(\gamma-1)(T_b+\bar{u}_0)} \right) Q_1 \\ = (\tfrac{1}{2}(\alpha_1^* \alpha_0^* + \beta_1^* \beta_0^*)(\gamma-1)^2 (T_b+\bar{u}_0)^2 (1-\bar{u}_0)^2 - \alpha_1^* \alpha_0^* (\gamma-1)(T_b+\bar{u}_0)(1-\bar{u}_0)^3) Q_0. \end{aligned} \tag{A 1d}$$

The homogeneous version of this equation, together with the conditions that $Q_1'(0) = 0$ and $Q_1 \to 0$ as $\xi \to \infty$, is simply the eigenvalue problem for (α_0^*, β_0^*); it follows that the inhomogeneous equation for Q_1 can only be solved if we now relax the condition on Q_1 at infinity. The appropriate solution of this equation which has $Q_1'(0) = 0$ is such that

$$Q_1 \sim Q_{1\infty} \quad \text{for} \quad \xi \gg 1,$$

where $Q_{1\infty}$ is a constant to be determined. If we denote the adjoint of Q_0 by Q_0^+ it follows that $Q_{1\infty}$ is given by

$$Q_{1\infty} = -2 \frac{\int_0^\infty (T_b+\bar{u}_0)(1-\bar{u}_0)^2 ((\alpha_1^* \alpha_0^* + \beta_1^* \beta_0^*)(\gamma-1)(T_b+\bar{u}_0) - 2\alpha_1^* \alpha_0^* (1-\bar{u}_0)) Q_0 Q_0^+ \, \mathrm{d}\xi}{\int_0^\infty (T_b+\bar{u}_0)(1-\bar{u}_0)^2 ((\alpha_0^{*2} + \beta_0^{*2})(\gamma-1)(T_b+\bar{u}_0) - 2\alpha_0^{*2}(1-\bar{u}_0)) Q_0^+ \, \mathrm{d}\xi}.$$

We have not computed $Q_{1\infty}$; however, because the eigenfunctions Q_0 have successively more oscillations in $(0, \infty)$ as α_0^* increases, we anticipate that for given (α_1^*, β_1^*), $Q_{1\infty}$ can be both positive and negative and will tend to zero when α_0^* becomes large.

For the scaling specified by (A 1*a*), region III of figure 4 has depth $\eta = O(M^{-\frac{3}{14}})$. The solution in this layer is calculated using the procedure outlined at the end of §3.1; the only significant change is that in matching regions III and IV we must now account for the fact that $Q_0 \sim \xi^{-7}$ for large ξ. After some manipulation we find that the eigenrelation obtained when this matching has been carried out is

$$\frac{1}{\hat{c}_1^{\frac{1}{4}}} + \frac{8\sqrt{2}}{3\sqrt{3}\pi} \frac{1}{\hat{c}_1^2} = \frac{1}{\hat{Q}_{1\infty}}, \tag{A 2a}$$

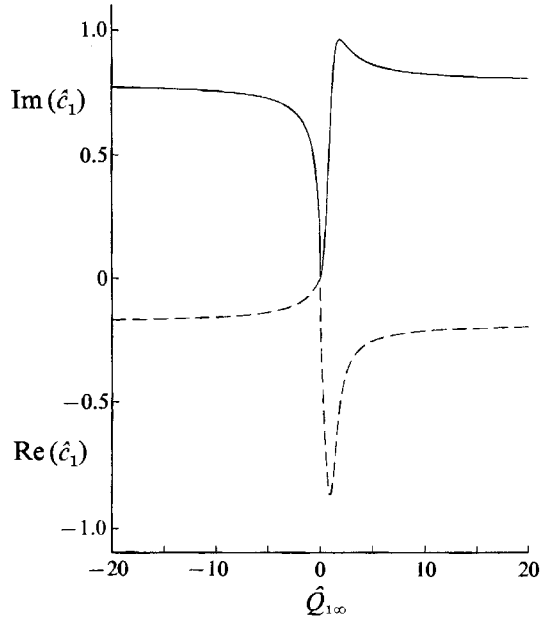

FIGURE 14. The real (– – –) and imaginary (——) parts of the solution of (A 2) for $-20 < \hat{Q}_{1\infty} < 20$.

where
$$\hat{Q}_{1\infty} = \frac{243\sqrt{3}\,\pi Q_{1\infty}}{7}(2(\alpha_0^{*2}+\beta_0^{*2}))^{\frac{15}{14}}. \tag{A 2b}$$

For a given real value of $\hat{Q}_{1\infty}$, this equation can be solved for $\hat{c}_1$; solutions are illustrated in figure 14. As expected by matching requirements, $\hat{c}_1$ approaches (3.13*b*) for large values of $|\hat{Q}_{1\infty}|$, while for small values of $\hat{Q}_{1\infty}$, $\hat{c}_1$ tends to zero. More precisely from (A 2) we find that for small $\hat{Q}_{1\infty}$

$$\hat{c}_1 \sim \left(\frac{8\sqrt{2}}{3\sqrt{3\pi}}\right)^{\frac{1}{2}}\hat{Q}_{1\infty}^{\frac{1}{2}} + \frac{1}{2}\left(\frac{8\sqrt{2}}{3\sqrt{3\pi}}\right)^{\frac{3}{8}}\hat{Q}_{1\infty}^{\frac{11}{8}} + \ldots, \tag{A 3}$$

so that, depending on the sign of $\hat{Q}_{1\infty}$, the growth rate goes to zero like $\hat{Q}_{1\infty}^{\frac{1}{2}}M^{-\frac{37}{14}}$ or $\hat{Q}_{1\infty}^{\frac{11}{8}}M^{-\frac{37}{14}}$. This behaviour is illustrated in figure 14 where we see that the slopes of the curves are discontinuous at the origin. This discontinuity can be smoothed out by considering an inner region. Indeed, we note from (A 3) that when $(\alpha-\alpha_0^*, \beta-\beta_0^*) = O(M^{-\frac{7}{2}})$, then $(1-c) = O(M^{-2})$; this turns out to be the appropriate scaling for almost neutral acoustic modes.

An asymptotic description of almost neutral acoustic modes has been given by CH and SB. Here we outline the analysis indicating the modifications due to the use of Sutherland's formula; in addition we identify the exact relationships with the long-wavelength vorticity mode.

For the almost neutral acoustic-mode scaling it is appropriate to expand the wavenumbers as

$$(\alpha,\beta) = \frac{1}{M^{\frac{3}{2}}}(\alpha_0^*,\beta_0^*) + \frac{1}{M^{2+\frac{\sqrt{7}}{2}}}(\alpha_1^*,\beta_1^*) + \ldots + \frac{1}{M^{\frac{7}{2}}}(\alpha_2^*,\beta_2^*) + \ldots, \tag{A 4a}$$

where the second term is forced by higher-order corrections to the mean flow, and only those terms we require have been displayed. In order to simplify the analysis we also slightly modify our definition of $\hat{c}_1$, etc., so that (cf. (3.15*a*))

$$c = 1+\frac{2}{(\gamma-1)(T_b+1)}\left(\frac{\hat{c}_1}{M^2}+\ldots+\frac{\hat{c}_2}{M^{\frac{7}{2}}}+\ldots\right). \tag{A 4b}$$

In the adjustment region, the velocity, temperature and pressure perturbation expand as

$$u = 1+\frac{2}{(\gamma-1)(T_b+1)}\left(\frac{\bar{G}}{M^2}+\ldots+\frac{\bar{G}_2}{M^{\frac{7}{2}}}+\ldots\right), \tag{A 5a}$$

$$T = (1-\bar{G})+\ldots-\bar{G}_2/M^{\frac{3}{2}}+\ldots, \quad \tilde{p} = \tilde{P}_0+\ldots+\tilde{P}_1/M^{\frac{3}{2}}+\ldots+\tilde{P}_2/M^3+\ldots, \tag{A 5b,c}$$

where the terms involving $\bar{G}_2$ are included for maximum generality. On substituting into (2.12*a*) and solving the resulting equations we find that $\tilde{P}_0$ is a constant, and

$$\tilde{P}_1' = -(1/\hat{c}_1^2)(\alpha_0^{*2}+\beta_0^{*2})^{\frac{1}{2}}(\bar{G}-\hat{c}_1)^2\tilde{P}_0, \tag{A 6a}$$

$$\tilde{P}_2' = (\alpha_0^{*2}+\beta_0^{*2})\left((\bar{G}-\hat{c}_1)^2\int^{\eta}\frac{(1-\bar{G})^2}{(\bar{G}-\hat{c}_1)^2}\,\mathrm{d}\eta-\frac{2(\bar{G}-\hat{c}_1)(\bar{G}_2-\hat{c}_2)}{\hat{c}_1^2(\alpha_0^{*2}+\beta_0^{*2})^{\frac{1}{2}}}\right)\tilde{P}_0, \tag{A 6b}$$

where $\tilde{P}_1'$ has been matched with the outer region where $\tilde{p}$ decays exponentially (i.e. where $\eta = O(M^{\frac{3}{2}})$).

In the high-temperature region where $\xi = O(1)$, the mean flow expands as

$$u = \bar{u}_0+\bar{u}_1/M^{\frac{1+\sqrt{7}}{2}}+\bar{u}_2/M^2+\ldots, \tag{A 7a}$$

while the appropriate expansion for the pressure perturbation is (cf. (A 1*b*)):

$$\tilde{p} = M^2Q_0+\ldots+M^{\frac{3-\sqrt{7}}{2}}Q_1+\ldots+Q_2+\ldots+Q_3/M^{\frac{3}{2}}+\ldots. \tag{A 7b}$$

Q_0 satisfies (3.14*b*), while Q_1 satisfies an inhomogeneous version of this equation (cf. (A 1*d*)). α_1^* is fixed by requiring that $Q_1'(0) = 0$ and $Q_1 \to 0$ as $\xi \to \infty$. Q_2 satisfies

$$\begin{aligned}
&Q_2''-\frac{2\bar{u}_0'}{\bar{u}_0-1}Q_2'-\tfrac{1}{4}(\gamma-1)^2(T_b+\bar{u}_0)^2(1-\bar{u}_0)^2\left((\alpha_0^{*2}+\beta_0^{*2})-\frac{2\alpha_0^{*2}(1-\bar{u}_0)}{(\gamma-1)(T_b+\bar{u}_0)}\right)Q_2\\
&-\tfrac{1}{2}(\alpha_2^*\alpha_0^*+\beta_2^*\beta_0^*)(\gamma-1)^2(T_b+\bar{u}_0)^2(1-\bar{u}_0)^2Q_0+\alpha_2^*\alpha_0^*(\gamma-1)(T_b+\bar{u}_0)(1-\bar{u}_0)^3Q_0\\
&-\tfrac{1}{2}(\alpha_0^{*2}+\beta_0^{*2})(\gamma-1)^2(T_b+\bar{u}_0)(1-\bar{u}_0)(1-T_b-2\bar{u}_0)\bar{u}_2Q_0\\
&-(\gamma-1)(T_b+\bar{u}_0)(1-\bar{u}_0)^2\alpha_0^{*2}(\bar{u}_2-\bar{c}_1)Q_0-\left(\frac{2\bar{u}_2'}{\bar{u}_0-1}-\frac{2\bar{u}_0'(\bar{u}_2-\bar{c}_1)}{(\bar{u}_0-1)^2}\right)Q_{0\xi}\\
&+(\tfrac{1}{2}(\gamma-1)(1-T_b-2\bar{u}_0)\bar{u}_2+1+(T_b-1)(1-\bar{u}_0))\alpha_0^{*2}(1-\bar{u}_0)^2Q_0\\
&-(\alpha_0^{*2}+\beta_0^{*2})(\gamma-1)(T_b+\bar{u}_0)(1-\bar{u}_0)(1+(T_b-1)(1-\bar{u}_0))Q_0 = 0,
\end{aligned} \tag{A 7c}$$

where

$$\bar{c}_j = \frac{2}{(T_b+1)(\gamma-1)}\hat{c}_j. \tag{A 7d}$$

For matching with (A 5*c*) we require that

$$Q_{2\infty} = \lim_{\xi\to\infty}Q_2 = \tilde{P}_0. \tag{A 8a}$$

Then, with the normalization that $q_0 = 1$ in (A 1c), we have from matching (A 6a) with (A 1c) that

$$\tilde{P}_0 = 7\hat{c}_1^2/1296(\alpha_0^{*2}+\beta_0^{*2})^{\frac{1}{2}},$$

and thus from (A 8a)

$$\hat{c}_1^2 = \tfrac{1296}{7}(\alpha_0^{*2}+\beta_0^{*2})^{\frac{1}{2}} Q_{2\infty}. \tag{A 8c}$$

From the form of (A 7c), we conclude that

$$\tfrac{1296}{7}(\alpha_0^{*2}+\beta_0^{*2})^{\frac{1}{2}} Q_{2\infty} = a_0\alpha_2^* + b_0\beta_2^* + 2d_0\hat{c}_1 + e_0, \tag{A 8d}$$

where a_0, b_0, d_0 and e_0 are all real constants which can be found numerically for a given choice of (α_0^*, β_0^*). It follows that

$$\hat{c}_1 = d_0 \pm (e_0 + d_0^2 + b_0\beta_2^* + a_0\alpha_2^*)^{\frac{1}{2}}. \tag{A 8e}$$

Hence if

$$a_0\alpha_2^* < -(e_0 + d_0^2 + b_0\beta_2^*), \tag{A 9a}$$

$\hat{c}_1$ is complex, and the appropriate choice of sign in (A 8e) is that which yields $\mathrm{Im}\,(\hat{c}_1) > 0$. As $|a_0\alpha_2^*| \to \infty$, a match with (A 3) is possible.

If

$$a_0\alpha_2^* \geqslant -(e_0 + d_0^2 + b_0\beta_2^*), \tag{A 9b}$$

then $\hat{c}_1$ is real, and it is necessary to calculate higher-order terms in order to identify the leading-order growth rate. To this end we hypothesize that $\mathrm{Im}\,(\hat{c}_2) \neq 0$; then the governing equation for Q_3 is

$$Q_3'' - \frac{2\bar{u}_0'}{\bar{u}_0 - 1}Q_3' - \tfrac{1}{4}(\gamma-1)^2(T_b+\bar{u}_0)^2(1-u_0)^2\left((\alpha_0^{*2}+\beta_0^{*2}) - \frac{2\alpha_0^{*2}(1-\bar{u}_0)}{(\gamma-1)(T_b+\bar{u}_0)}\right)Q_3$$

$$= \left(\frac{2\bar{u}_0'}{(\bar{u}_0-1)^2}Q_{0\xi} - (\gamma-1)(T_b+\bar{u}_0)(1-\bar{u}_0)^2\alpha_0^{*2}Q_0\right)\bar{c}_2 + \ldots, \tag{A 10a}$$

where only those terms that force the complex part of the eigenfunction have been displayed. From (A 7c) and (A 8d) we conclude that

$$\tfrac{1296}{7}(\alpha_0^{*2}+\beta_0^{*2})^{\frac{1}{2}}\,\mathrm{Im}\,(Q_{3\infty}) = 2d_0\,\mathrm{Im}\,(\hat{c}_2). \tag{A 10b}$$

From matching with (A 5c) it follows that

$$\mathrm{Im}\,(\tilde{P}_1) = \frac{7}{648(\alpha_0^{*2}+\beta_0^{*2})^{\frac{1}{2}}}d_0\,\mathrm{Im}\,(\hat{c}_2), \tag{A 10c}$$

and then after matching both $\tilde{P}_1$ and $\tilde{P}_2$ with the exponentially decaying pressure in outer region I, we conclude that

$$\mathrm{Im}\,(\tilde{P}_2') \to -\tfrac{7}{648}d_0\,\mathrm{Im}\,(\hat{c}_2) \quad \text{as} \quad \eta \to \infty. \tag{A 10d}$$

In the case of the Chapman viscosity law, CH showed that a similar matching argument generates two terms on the right-hand side of the equivalent expression to (A 10d).

Next we note from (A 6b) that if the integral is complex as $\eta \to 0$, then it will force an $O(M^{\frac{1}{2}})$ complex term in (A 7b). In turn this will lead to an $O(M^{-\frac{7}{2}})$ term by interaction with the basic velocity profile (A 7a), but this complex term is larger in magnitude than the $O(M^{-\frac{3}{2}})$ term supposed to be the largest complex term in (A 7b). We conclude by contradiction that the integral in (A 6b) must be real as $\eta \to 0$.

As in CH and SB, since $\hat{c}_1$ is real, there is a critical layer at η_c, defined as where $\bar{G}_c = \hat{c}_1$ (the subscript c indicates evaluation at η_c). This generates a complex

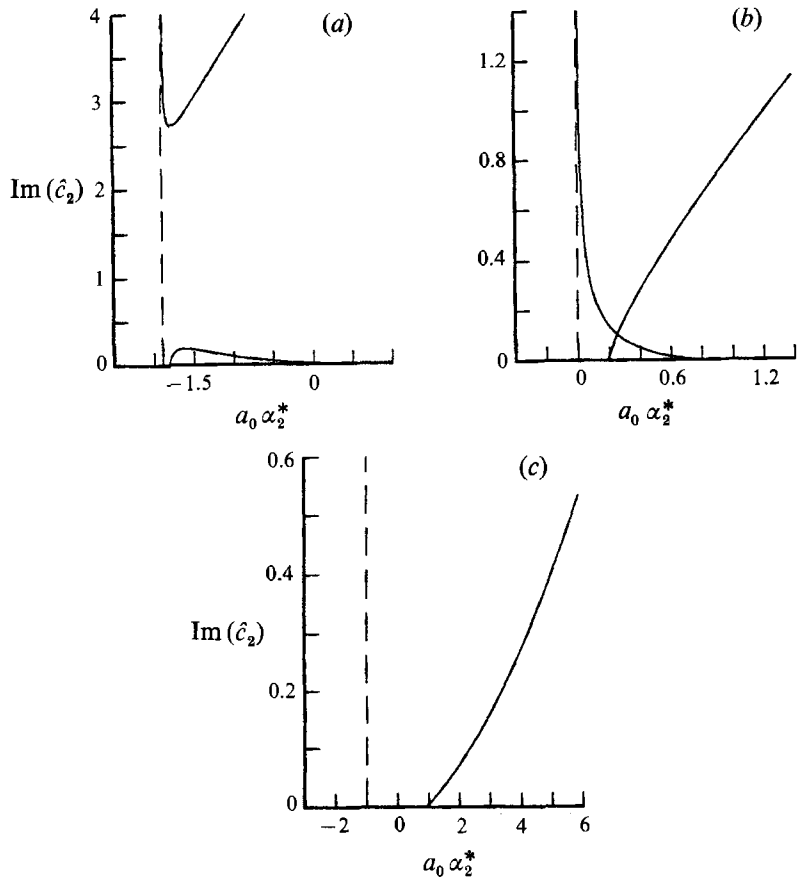

FIGURE 15. Schematic illustration of the growth rate in the immediate neighbourhood of an acoustic-mode eigenvalue. The three generic types of behaviour are illustrated: (*a*) $d_0 < \hat{c}_{1s} < 0$, (*b*) $\hat{c}_{1s} < d_0 < 0$, and (*c*) $\hat{c}_{1s} < 0 < d_0$.

contribution to the integral in (A 6*b*) for $\eta > \eta_c$. Hence from (A 6*b*), (A 10*b*), and the standard formulae for jumps across linear critical layers where Im $(c) > 0$, it follows that

$$(\hat{c}_1 - d_0)\,\mathrm{Im}\,(\hat{c}_2) = -\tfrac{1}{2}\pi(\alpha_0^{*2}+\beta_0^{*2})^{\frac{1}{2}}\hat{c}_1^4(1-\bar{G}_c)\left(\frac{2\bar{G}_c'^2+(1-\bar{G}_c)\bar{G}_c''}{\bar{G}_c'^3}\right). \qquad \text{(A 11)}$$

In the limit when $\hat{c}_1 \ll -1$, (A 11) can be shown to match with the second-order term in (A 3). Also, as $\hat{c}_1 \to d_0$, Im $(\hat{c}_2) \to \infty$, with the result that a match can in principle be made with (A 8*e*); although strictly a further subregion needs to be considered for the match to be made perfect.

The nature of solutions to (A 8*e*) and (A 11) depends on the relative magnitudes of the real constant d_0, and the scaled velocity at the generalized inflexion point, i.e. $\hat{c}_{1s}$. Rather than calculate d_0 for many different velocity profiles, here we outline the three types of generic behaviour that can occur.

(*a*) If $d_0 < \hat{c}_{1s} < 0$, then a plot of Im $(\hat{c}_2)$ against $a_0\alpha_2^*$ is as shown schematically in figure 15(*a*). The dashed line indicates the value of $a_0\alpha_2^*$ at which $\hat{c}_1 = d_0$. There are two independent branches corresponding to the two choices of sign in (A 8*e*); one of these is the continuation of the long-wavelength vorticity mode, while the other is a

small-growth-rate acoustic mode. For the first eigenvalue given by (3.15*b*), numerical evaluation yields $d_0 = -2.23$. Since $\hat{c}_{1s} = -0.99$ an independent small-growth-rate acoustic mode is predicted. This is confirmed by the full numerical solutions of Rayleigh's equation for $M = 20$ reported in §6.

(*b*) If $\hat{c}_{1s} < d_0 < 0$, then there are again two independent branches corresponding to the two choices of sign in (A 8*e*) – see figure 15(*b*). However, now there is no independent small-growth-rate acoustic mode; instead one branch of the long-wavelength vorticity modes terminates as an inflexion-point neutral mode, while the other terminates as a free-stream neutral mode. If $\hat{c}_{1s} < 2d_0$, then the two modes do not overlap in the wavenumber range, and there is a narrow range of wavenumbers for which there is no growing mode.

(*c*) If $\hat{c}_{1s} < 0 < d_0$, the negative sign in (A 8*e*) is appropriate and there is only one identifiable branch for which $\mathrm{Im}(\hat{c}_2) = O(1)$ (see figure 15*c*); there is of course another branch for which $\mathrm{Im}(\hat{c}_1) = O(1)$. Again there is no independent small-growth-rate acoustic mode. One branch of the long-wavelength vorticity mode terminates as an inflexion-point neutral mode, while the other terminates as a neutral mode with a wave speed greater than that of the free stream (as $d_0 > 0$). In the latter case, the lack of a critical layer means that the leading-order growth rate is essentially given by (A 8*e*) right up to the neutral point. There is a narrow range of wavenumbers for which there is no growing mode. In unscaled variables this gap is very narrow.

Finally, we note the differences to the above results if we had considered spatial rather than temporal stability. As in §3.1 simplifications arise because on the almost-neutral acoustic-mode scaling the waves travel at approximately the free-stream velocity. Therefore, writing

$$\omega = (1+\tilde{c})\,\alpha, \tag{A 12a}$$

Rayleigh's equation becomes

$$\frac{\mathrm{d}^2\tilde{p}}{\mathrm{d}\eta^2} - \frac{2\bar{u}'}{\bar{u}-1-\tilde{c}}\frac{\mathrm{d}\tilde{p}}{\mathrm{d}\eta} - T\left(\left[\left(\frac{\omega}{1+\tilde{c}}\right)^2+\beta^2\right]T - \left(\frac{\omega}{1+\tilde{c}}\right)^2 M^2(\bar{u}-1-\tilde{c})^2\right)\tilde{p} = 0. \tag{A 12b}$$

On expanding for small $\tilde{c}$, the leading-order equation is formally the same as for the temporal stability case if we identify ω and α. As a result the equations in the adjustment layer and the exponentially decaying region do not change to the order calculated. However, in the high-temperature boundary layer, the forcing terms for Q_2 and Q_3 are affected. Suppose that, based on (A 4*a*), we expand the frequency as

$$\omega = \frac{1}{M^{\frac{3}{2}}}\omega_0^* + \frac{1}{M^{2+\frac{\sqrt{7}}{2}}}\omega_1^* + \ldots + \frac{1}{M^{\frac{7}{2}}}\omega_2^* + \ldots, \tag{A 12c}$$

then the term

$$(\gamma-1)\,(T_{\mathrm{b}}+\bar{u}_0)\,(1-\bar{u}_0)^2((1-\bar{u}_0)-\tfrac{1}{2}(\gamma-1)\,(T_{\mathrm{b}}+\bar{u}_0))\,Q_0\,\omega_0^{*2}\bar{c}_1$$

needs to be added to the right-hand side of the equation for Q_2, i.e. (A 7*c*); similarly for Q_3. The effect of this is to change the coefficients for $\hat{c}_1$ and $\hat{c}_2$ in (A 8*d*) and (A 10*b*) respectively; we denote this new coefficient by $\tilde{d}_0$. The dispersion relations (A 8*e*) and (A 11) are then unchanged except for the substitution of $\tilde{d}_0$ for d_0. In particular, if the abscissa in figure 15 is interpreted as the scaled frequency, then the three generic types of behaviour illustrated can still occur.

The value of $\tilde{d}_0$ can thus have an important effect on a fixed-frequency disturbance travelling downstream. If we assume that such a disturbance remains linear (despite its exponential growth), then its scaled frequency, ω, changes as the boundary layer

thickens. If $\tilde{d}_0 < \hat{c}_{1s}$ (figure 15*a*), then a long-wavelength vorticity mode excited upstream will still exist after the scaled frequency has passed through one of the eigenvalues (3.15*b*), although the spatial growth rate will have decreased temporally at the eigenvalue. However, if $\tilde{d}_0 > \hat{c}_{1s}$, then close to the eigenvalue the growth rate decreases to zero, with the result that the mode will have to be re-excited if it is to occur further downstream. We note that because of the existence of a critical layer at the eigenvalues, nonlinear effects may have an enhanced significance as the disturbance evolves through these specific wavenumbers (cf. Goldstein & Wundrow 1990, and see the recent work of Wundrow 1992).

REFERENCES

Abramowitz, M. & Stegun, I. A. 1964 *Handbook of Mathematical Functions*. National Bureau of Standards.

Balsa, T. F. & Goldstein, M. E. 1990 On the instabilities of supersonic mixing layers: a high Mach number asymptotic theory. *J. Fluid Mech.* **216**, 585–611.

Blackaby, N. D. 1991 On viscous, inviscid and centrifugal instability mechanisms in compressible boundary layers, including non-linear vortex/wave interaction and the effects of large Mach number on transition. Ph.D. thesis, University of London.

Brown, S. N., Khorrami, A. F., Neish, A. & Smith, F. T. 1991 On hypersonic boundary-layer interactions and transition. *Phil. Trans. R. Soc. Lond.* A **335**, 139–152.

Brown, S. N. & Stewartson, K. 1975 A non-uniqueness of the hypersonic boundary layer. *Q. J. Mech. Appl. Maths* **XXVIII**, 75–90.

Bush, W. B. 1966 Hypersonic strong similarity solutions for flow past a flat plate. *J. Fluid Mech.* **25**, 51–64.

Bush, W. B. & Cross, A. K. 1967 Hypersonic weak interaction similarity solutions for flow past a flat plate. *J. Fluid Mech.* **29**, 349–359.

Cowley, S. J. & Hall, P. 1990 On the instability of flow past a wedge. *J. Fluid Mech.* **214**, 17–43 (referred to herein as CH).

Dunn, D. W. & Lin, C. C. 1955 On the stability of the laminar boundary layer in a compressible fluid. *J. Aero. Sci.* **22**, 455–477.

Fischer, M. C. & Weinstein, L. M. 1972 Cone transitional boundary-layer structure at $M_e = 14$. *AIAA J.* **10**, 699–701.

Freeman, N. C. & Lam, S. H. 1959 On the Mach number independence principle for a hypersonic boundary layer. *Princeton University Rep.* 471.

Fu, Y., Hall, P. & Blackaby, N. D. 1990 On the Görtler instability in hypersonic flows: Sutherland law fluids and real gas effects. *ICASE Rep.* 90-85; and to appear in *Phil. Trans. R. Soc. Lond.* A.

Gajjar, J. S. B. & Cole, J. W. 1989 Upper branch stability of compressible boundary layer flows. *Theor. Comput. Fluid Dyn.* **1**, 105–123.

Goldstein, M. E. & Wundrow, D. W. 1990 Spatial evolution of nonlinear acoustic mode-instabilities on hypersonic boundary layers. *J. Fluid Mech.* **219**, 585–607.

Grubin, S. E. & Trigub, V. N. 1993*a* The asymptotic theory of a hypersonic boundary layer stability. *J. Fluid Mech.* **246**, 361–380.

Grubin, S. E. & Trigub, V. N. 1993*b* The long-wave limit in the asymptotic theory of a hypersonic boundary layer stability. *J. Fluid Mech.* **246**, 381–395.

Hall, P. & Fu, Y. 1989 Görtler vortices at hypersonic speeds. *Theor. Comput. Fluid Mech.* **1**, 125–134.

Hall, P. & Smith, F. T. 1991 On strongly nonlinear vortex/wave interactions in boundary-layer transition. *J. Fluid Mech.* **227**, 641.

Heisenberg, W. 1924 Über Stabilität und Turbulenz von Flussigkeitsströmen. *Ann. Phys. Lpz.* (4) **74**, 577–627.

Jackson, T. L. & Grosch, C. E. 1989 Inviscid spatial instability of a compressible mixing layer. *J. Fluid Mech.* **208**, 609–638.

JACKSON, T. L. & GROSCH, C. E. 1991 Inviscid spatial instability of a compressible mixing layer. Part 3. *J. Fluid Mech.* **224**, 159–175.

LEE, R. S. & CHENG, H. K. 1969 On the outer edge problem of a hypersonic boundary layer. *J. Fluid Mech.* **38**, 161–179.

LEES, L. 1953 On the boundary layer equations in hypersonic flow and their approximate solutions. *J. Aero. Sci.* **30**, 143–145.

LEES, L. & LIN, C. C. 1946 Investigation of the stability of the laminar boundary layer in a compressible fluid. *NACA Tech. Note* 1115.

LIN, C. C. 1945*a* On the stability of two-dimensional parallel flows, Part I. *Q. Appl. Maths.* **3**, 117–142.

LIN, C. C. 1945*b* On the stability of two-dimensional parallel flows, Part II. *Q. Appl. Maths* **3**, 218–234.

LIN, C. C. 1945*c* On the stability of two-dimensional parallel flows, Part III. *Q. Appl. Maths* **3**, 277–301.

LUNIEV, V. V. 1959 On the similarity of hypersonic viscous flows around slender bodies. *Prikl. Mat. Mech.* **23**, 193–197.

MACK, L. M. 1969 Boundary-layer stability theory. *Document* 900-277. *Rev. A.* Jet Propulsion Laboratory, Pasadena, CA.

MACK, L. M. 1984 Boundary-layer linear stability theory. In *Special Course on Stability and Transition of Laminar Flow. AGARD* Rep. 709.

MACK, L. M. 1987 Review of linear compressible stability theory. In *Stability of Time Dependent and Spatially Varying Flows*, (ed. D. L. Dwoyer & M. Y. Hussaini). Springer.

MALMUTH, N. D. 1991 Inviscid stability of hypersonic strong interaction flow over a flat plate. *J. Fluid Mech.* (submitted).

PAPAGEORGIOU, D. T. 1990 Linear instability of the supersonic wake behind a flat plate aligned with a uniform stream. *Theor. Comput. Fluid Dyn.* **1**, 327–348.

PAPAGEORGIOU, D. T. 1991 The stability of two-dimensional wakes and shear-layers at high Mach numbers. *Phys. Fluids* A **3**, 793–802.

RESHOTKO, E. 1976 Boundary-layer stability and transition. *Ann. Rev. Fluid Mech.* **8**, 311–350.

RESHOTKO, E. & KHAN, M. M. S. 1979 Stability of the laminar boundary layer on a blunted plate in supersonic flow. In *IUTAM Symp. Stuttgart, Germany on Laminar-Turbulent Transition.* Springer.

RYZHOV, O. S. 1984 Stability and separation of viscous flows. In *IUTAM Symp. Novosibirsk, USSR on Laminar–Turbulent Transition.* Springer.

SEDDOUGUI, S. O. & BASSOM, A. P. 1991 Nonlinear instability of hypersonic flow past a wedge. *Theor. Comput. Fluid Dyn.* (submitted).

SEDDOUGUI, S. O., BOWLES, R. I. & SMITH, F. T. 1991 Surface-cooling effects on compressible boundary layer instability. *Eur. J. Mech.* B/*Fluids* **10**, 117–145.

SMITH, F. T. 1979 On the non-parallel flow stability of the Blasius boundary layer. *Proc. R. Soc. Lond.* A **366**, 91–109.

SMITH, F. T. 1989 On the first-mode instability in subsonic, supersonic or hypersonic boundary layers. *J. Fluid Mech.* **198**, 127–154.

SMITH, F. T. & BROWN, S. N. 1990 The inviscid instability of a Blasius boundary layer at large values of the Mach number. *J. Fluid Mech.* **219**, 499–518 (referred to herein as SB).

STEWARTSON, K. 1955 On the motion of a flat plate at high speed in a viscous compressible fluid – II. Steady motion. *J. Aero. Sci.* **22**, 303–309.

STEWARTSON, K. 1964 *Theory of Laminar Boundary Layers in Compressible Fluids.* Oxford University Press.

TOLLMIEN, W. 1929 Über die Entstehung der Turblenz. *Nachr. Ges. Wiss. Göttingen, Math.-Phys. Klasse*, 21–44.

WUNDROW, D. W. 1992 Nonlinear spatial evolution of inviscid instabilities on hypersonic boundary layers. *J. Fluid Mech.* (in press).